JUSTC

Article

http://justc.ustc.edu.cn

Received: November 27, 2023; Accepted: February 28, 2024

On joint analysing *XMM-NuSTAR* spectra of active galactic nuclei

Jia-Lai Kang[1,2] ✉, and Jun-Xian Wang[1,2] ✉

[1]*CAS Key Laboratory for Research in Galaxies and Cosmology, Department of Astronomy, University of Science and Technology of China, Hefei 230026, China;*
[2]*School of Astronomy and Space Science, University of Science and Technology of China, Hefei 230026, China*

✉Correspondence: Jia-Lai Kang, E-mail: ericofk@mail.ustc.edu.cn; Jun-Xian Wang, E-mail: jxw@ustc.edu.cn

Graphical abstract

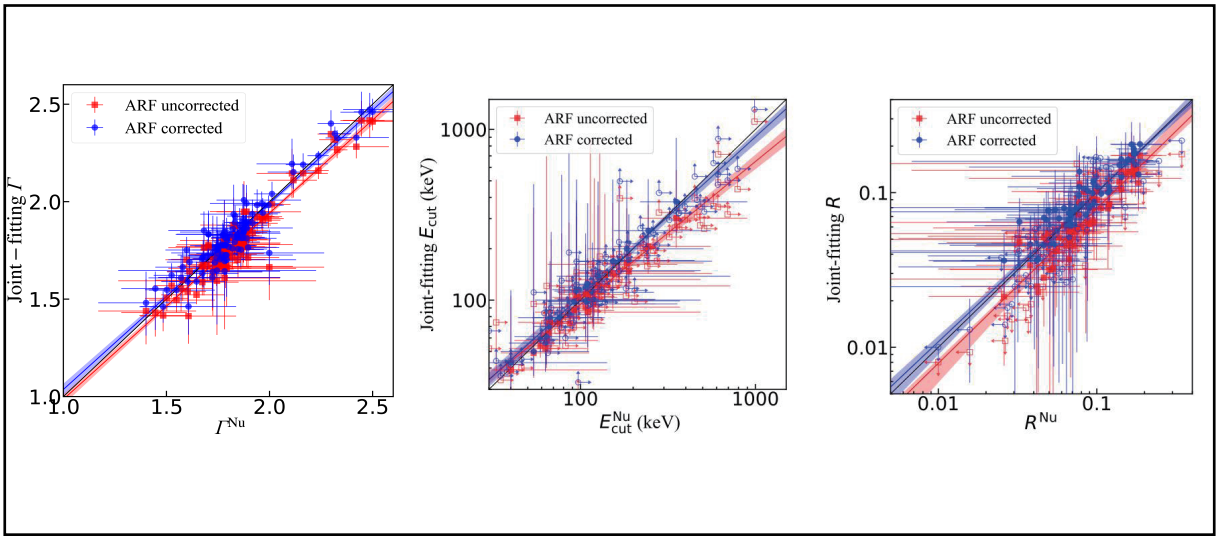

Γ, E_{cut}, and R derived through fitting the NuSTAR spectra alone versus joint-fitting XMM-NuSTAR spectra (before/after the ARF correction).

Public summary

- In this work, we perform joint-fitting of *NuSTAR* and EPIC-pn spectra for a large sample of 104 observation pairs of 44 X-ray bright AGN. EPIC-pn spectra are systematically more difficult than those of *NuSTAR* ($\Delta\Gamma \sim 0.1$), leading to an underestimated of the cutoff energy $E_{\rm cut}$ and the reflection component R when performing joint-fitting before correcting the calibration issue.

- The empirical correction of the effective area implemented in latest *XMM-Newton* calibration files (but would not be applied by default) is highly effective and could commendably erase the discrepancy in the derived best-fit Γ, $E_{\rm cut}$, and R.

- For this sample, requiring perfect simultaneity between the *NuSTAR* and EPIC-pn spectra leads to severse loss of the net exposure time of *NuSTAR*. Consequently, fitting *NuSTAR* spectra jointly with simultaneous EPIC-pn data does not always improve the constraints on the key spectral parameters.

- For *XMM-Newton* EPIC-pn observations in small window (SW) mode, insufficient filtering of high background flares could bias the spectral fitting results due to the background vignetting effect, which is no longer negligible in case of background flares. A threshold of 0.05 counts/s to filter background flares appears appropriate for EPIC-pn SW mode.

Citation: Kang J L, Wang J X. On joint analysing *XMM-NuSTAR* spectra of active galactic nuclei. *JUSTC*, **2024**, 54(7): 0702. DOI: 10.52396/JUSTC-2023-0160

JUSTC

Article

http://justc.ustc.edu.cn

Received: November 27, 2023; Accepted: February 28, 2024

On joint analysing *XMM-NuSTAR* spectra of active galactic nuclei

Jia-Lai Kang[1,2] ✉, and Jun-Xian Wang[1,2] ✉

[1]*CAS Key Laboratory for Research in Galaxies and Cosmology, Department of Astronomy, University of Science and Technology of China, Hefei 230026, China;*
[2]*School of Astronomy and Space Science, University of Science and Technology of China, Hefei 230026, China*

✉Correspondence: Jia-Lai Kang, E-mail: ericofk@mail.ustc.edu.cn; Jun-Xian Wang, E-mail: jxw@ustc.edu.cn

Cite This: *JUSTC*, **2024**, 54(7): 0702 (15pp)

Read Online

Abstract: A recently released *XMM-Newton* note revealed a significant calibration issue between nuclear spectroscopic telescope array (*NuSTAR)* and *XMM-Newton* European Photon Imaging Camera (EPIC) and provided an empirical correction to the EPIC effective area. To quantify the bias caused by the calibration issue in the joint analysis of *XMM-NuSTAR* spectra and verify the effectiveness of the correction, in this work, we perform joint-fitting of the *NuSTAR* and EPIC-pn spectra for a large sample of 104 observation pairs of 44 X-ray bright active galactic nuclei (AGN). The spectra were extracted after requiring perfect simultaneity between the *XMM-Newton* and *NuSTAR* exposures (merging Good Time Intervals, GTIs from two missions) to avoid bias due to the rapid spectral variability of the AGN. Before the correction, the EPIC-pn spectra are systematically harder than the corresponding *NuSTAR* spectra by $\Delta\Gamma \sim 0.1$, subsequently yielding significantly underestimated cutoff energy $E_{\rm cut}$ and the strength of reflection component R when performing joint-fitting. We confirm that the correction is highly effective and can commendably erase the discrepancy in best-fit Γ, $E_{\rm cut}$, and R. We thus urge the community to apply the correction when joint-fitting *XMM-NuSTAR* spectra, but note that the correction is limited to 3–12 keV and therefore not applicable when the soft X-ray band data are included. Besides, we show that as merging GTIs from two missions would cause severe loss of *NuSTAR* net exposure time, in many cases, joint-fitting yields no advantage compared with utilizing *NuSTAR* data alone. We finally present a technical note on filtering periods of high background flares for *XMM-Newton* EPIC-pn exposures in the Small Window mode.

Keywords: active galactic nuclei; X-ray spectroscopy; *XMM-Newton*; *NuSTAR*; cross-calibration issue

CLC number: P141.5 **Document code:** A

1 Introduction

The nuclear spectroscopic telescope array (*NuSTAR*)[1], the first direct-imaging hard X-ray mission with a spectral coverage from 3 keV to 79 keV, has remarkably boosted the study of various high-energy phenomena. Active galactic nuclei (AGN) are the dominant population in the extragalactic X-ray sky. According to the widely accepted disk-corona paradigm, the primary X-ray emission of AGN originates in a hot and compact region, namely the corona[2, 3]. The seed photons from the accretion disk are upscattered to the X-ray band through inverse Comptonization, producing the observed power-law continuum, with a cutoff at the high-energy end, which is a direct indicator of the coronal temperature $T_{\rm e}$. For AGN studies, *NuSTAR* opens a new window to detect/measure the X-ray high-energy cutoff $E_{\rm cut}$ (and effectively, the corona temperature $T_{\rm e}$) in many sources[4–9]. Meanwhile, *NuSTAR* observations are also essentially helpful for constraining the reflection component in the X-ray spectra[10–13].

In practice, *NuSTAR* data are often analyzed in association with the coordinated data of other X-ray missions, to achieve a broader energy coverage and a higher spectral signal-to-noise ratio at < 10 keV, which could supposedly improve the constraints on X-ray spectral parameters. Among the coordinated missions, *XMM-Newton*[14] is of most significance, with the longest coordinated observing time since the *NuSTAR* Cycle 2①. Due to the large effective areas of the European Photon Imaging Cameras (EPIC), *XMM-Newton* could provide high-quality spectra at 0.3–10 keV, potentially as an effective complement to *NuSTAR*.

However, proper inter-instrument calibration is critical prior to analyzing joint observations from different observatories. A possible calibration issue between *NuSTAR* and *XMM-Newton* has been reported in the literature[15–17]. Such calibration issues could be the fundamental cause of the descrepancy in the measurements of $E_{\rm cut}$ or $T_{\rm e}$ in individual AGN, between studies fitting *NuSTAR* spectra alone [7, 9, 18–22], and those joint-fitting quasi-simultaneous data from other missions[8, 23–29].

The calibration issue between *NuSTAR* and *XMM-Newton* was confirmed by a recently released *XMM-Newton* calibration technical note②, in which the EPIC-pn spectra of the Crab Nebula were found to be systematically harder than those of

① https://heasarc.gsfc.nasa.gov/docs/nustar/nustar_prop.html
② https://xmmweb.esac.esa.int/docs/documents/CAL-TN-0230-1-3.pdf

DOI: 10.52396/JUSTC-2023-0160
JUSTC, **2024**, 54(7): 0702

NuSTAR, with $(\Gamma^{\rm pn}-\Gamma^{\rm NuSTAR})\sim-0.1$. Basically, the calibration of *NuSTAR* is supposed to be more reliable thanks to a novel approach of observing the Crab through stray-light, which avoids the uncertainties caused by the X-ray optics[30, 31]. Therefore, *XMM-Newton* has implemented an empirical correction of the effective area of EPIC based on *NuSTAR* results after SAS 20.0 in the newest *XMM-Newton* calibration files①, improving the cross-calibration with *NuSTAR*. Such a correction, limited to 3–12 keV and thus not deployed by default in the pipeline, has not been adopted by most joint-analyses of *XMM-NuSTAR* spectra of AGN in literature. It is both technically and scientifically important to investigate how this calibration issue biases the X-ray spectral measurements of AGN, verify the effectiveness of the correction, and if yes, provide the updated X-ray spectral parameters after applying the calibration correction for AGN with joint *XMM-NuSTAR* observations.

2 Sample and data reduction

We match the 817 Seyfert galaxies in the 105 month *Swift*/BAT catalog[32] with archival *NuSTAR* and *XMM-Newton* observations (as of 2023 August). In this work we focus on the EPIC-pn data of *XMM-Newton*[33], which are most widely used in literature. However, the empirical correction of the effective areas for *XMM-Newton* EPIC-MOS[34] is exactly the same (see the calibration note①), so the conclusions about the cross-calibration should also apply to the MOS data. We searched for simultaneous observation pairs of the two missions, requiring an overlapping exposure time > 5 ks between *NuSTAR* and EPIC-pn, obtaining 176 observation pairs of 94 sources. Note that one *NuSTAR* exposure may overlap in time with more than one *XMM-Newton* exposure, and vice versa. Observation pairs with too few counts, serious absorption with $N_{\rm H}>10^{23}$ cm^{-2}, or complicated spectra badly fitted (χ^2/dof > 1.2) with the model in Kang and Wang[9], are further dropped, resulting in a final sample of 104 observation pairs (consisting of 100 *NuSTAR* and 102 *XMM-Newton* observations) of 44 sources (see Table 1)②.

The raw *NuSTAR* data are reduced with the *nupipeline*, which is part of the HEASoft package (version 6.32.1), with calibration files of version 20210824. We extract the *NuSTAR* spectra using *nuproducts*, adopting a circular source region with a radius of 60 arcsec for each source, and an annulus from 120 arcsec to 150 arcsec for background extraction. Raw *XMM-Newton* data are processed with the Science Analysis Software (SAS 20.0.0) and current calibration files (CCF 3.13). We extract the source spectra from a circular region, the radius of which is optimally determined by *eregionanalyse*, with background from nearby source-free regions (see Fig. 1). *epatplot* is employed to confirm that the pile-up effect is negligible in all the observations. Specifically, the observed-to-model fractions of single and double events at 3–10 keV are consistent with 1.0 at the 3σ confidence level in most observations (88 out of 102), while the deviations from 1.0 for the other 14 observations are all smaller than 5%. Two ancillary response files (ARF) are created for each observation, with/without applying the aforementioned empirical correction of the effective area, by setting the parameter *applyabsfluxcorr* of the task *arfgen*. Finally, all the spectra are rebinned to attain a minimum of 50 counts per bin using *grppha*.

In the above paragraph, we describe a typical data reduction process, but omit an ambiguous step of reducing the *XMM-Newton* data, i.e., filtering periods suffering from the flaring background. Solar protons could produce flaring EPIC background, which is highly unpredictable and affects a large fraction of *XMM-Newton* observation time[35, 36]. As recommended by the user guide③, a viable method is to extract a rate curve (usually with a time bin <= 100 s) in the source-free regions, of only valid single events with energy between 10 keV and 12 keV ("PATTERN==0 && PI IN [10000：12000]" in the expression of *evselect*). A new good time interval (GTI) file will then be generated, dropping the periods with count rate above certain threshold, a recommended value of which is 0.4 counts/s for the EPIC-pn camera in the full frame mode (hereafter FF mode).

However, as shown in Table 1, most observations (85/102) of these bright AGN are operated in the small window mode (hereafter SW mode) to avoid serious pile-up effect, which has a much smaller (1/36) field of view (FOV) than the FF mode. The value of the count rate threshold is hence supposed to be smaller for the SW mode, while the time bin of the rate curve should be large enough to contain sufficient counts. Therefore, for these SW observations, we try three different thresholds: (ⅰ) 0.4 counts/s, the same as in the FF mode; (ⅱ) 0.008 counts/s, scaled down because in the SW mode a much smaller sky area (see Fig. 1) could be used to extract 10–12 keV light curve for high background filtering; and (ⅲ) 0.05 counts/s, a moderate threshold between (ⅰ) and (ⅱ); and adopt a time bin of 500 s. The consequent usable fraction of GTI is shown in Fig. 2. Apparently, the threshold of 0.008 counts/s is too strict, leading to less than 40% GTI usable in more than half of the observations. Meanwhile, the threshold of 0.4 counts/s is likely too loose, causing insufficient filtering, the bias of which we shall show in Section 4.2. On the other hand, the threshold of 0.05 counts/s seems to be reasonable, and the corresponding distribution of usable GTI is similar to the one in Read and Ponman[35], of a detailed study of EPIC background with FF observations.

Therefore, in our analyses below we adopt a threshold of 0.05 counts/s (unless otherwise stated, see the lower panel of Fig. 3 for an example) to filter the flaring background for SW observations④, while in Section 4.2, using *NuSTAR* spectra as reference, we shall show that such a threshold is indeed appropriate, whereas a looser threshold (0.4 counts/s) will lead

① See the introduction in the CCF release note: https://xmmweb.esac.esa.int/docs/documents/CAL-SRN-0388-1-4.pdf

② 21 observation pairs in this work were also adopted in the aforementioned technical note, but only used to show the improvement of the statistics (reduction of χ^2), irrelevant to the derivation of the empirical correction of ARF. We confirm the inclusion of these observations in this work does not bias our analysis

③https://xmm-tools.cosmos.esa.int/external/xmm_user_support/documentation/sas_usg/USG/epicbkgfiltering.html

④ We adopt a threshold of 0.4 counts/s and 0.2 counts/s, for FF and LW observations respectively. The sample of them is too small to perform similar analysis.

DOI: 10.52396/JUSTC-2023-0160
JUSTC, **2024**, 54(7): 0702

Table 1. Fitting results of *NuSTAR*, *XMM*, and joint spectra (requiring perfect simultaneity between *NuSTAR* and *XMM* exposures)

Source	Nu ID	XMM ID	Mode	$N_{\rm H}^{\rm Nu}$ $10^{22}{\rm cm}^{-2}$	$N_{\rm H}^{\rm pn}$ $10^{22}{\rm cm}^{-2}$	$N_{\rm H}^{\rm pn-Cor}$ $10^{22}{\rm cm}^{-2}$	$\Gamma^{\rm Nu}$	$\Gamma^{\rm pn}$	$\Gamma^{\rm pn-Cor}$	$\Gamma^{\rm joint}$	$\Gamma^{\rm joint-Cor}$	$E_{\rm cut}^{\rm Nu}$ (keV)	$E_{\rm cut}^{\rm joint}$ (keV)	$E_{\rm cut}^{\rm joint-Cor}$ (keV)	$R^{\rm Nu}$	$R^{\rm joint}$	$R^{\rm joint-Cor}$
Fairall 9	60001130002	07413301	SW	<1.90	<2.67	<3.05	$1.78^{+0.16}_{-0.21}$	$1.86^{+0.22}_{-0.20}$	$1.97^{+0.24}_{-0.20}$	$1.80^{+0.20}_{-0.17}$	$1.84^{+0.17}_{-0.15}$	>38	>37	>38	<1.05	<1.34	<1.67
Mrk 359	60402021004	08305509	SW	<0.98	<0.38	<0.43	$1.84^{+0.14}_{-0.12}$	$1.71^{+0.09}_{-0.09}$	$1.79^{+0.09}_{-0.09}$	$1.77^{+0.09}_{-0.09}$	$1.82^{+0.10}_{-0.09}$	>95	>89	>99	$0.85^{+0.97}_{-0.58}$	$0.56^{+0.72}_{-0.44}$	$0.72^{+0.79}_{-0.46}$
	60402021006	08305510	SW	<1.06	<0.39	<0.45	$1.84^{+0.04}_{-0.11}$	$1.75^{+0.09}_{-0.09}$	$1.82^{+0.09}_{-0.08}$	$1.79^{+0.08}_{-0.08}$	$1.83^{+0.08}_{-0.08}$	>109	>112	>125	$0.53^{+0.72}_{-0.43}$	$0.32^{+0.56}_{-0.31}$	$0.47^{+0.59}_{-0.35}$
	60402021008	08305511	SW	<3.25	<0.88	<1.02	$1.78^{+0.27}_{-0.24}$	$1.50^{+0.10}_{-0.09}$	$1.57^{+0.10}_{-0.08}$	$1.61^{+0.13}_{-0.26}$	$1.64^{+0.20}_{-0.15}$	>65	>52	>49	<1.97	<1.02	<1.19
NGC 931	60101002002	07605302	LW	$0.80^{+0.62}_{-0.72}$	<0.77	$0.75^{+0.40}_{-0.40}$	$1.88^{+0.07}_{-0.08}$	$1.75^{+0.05}_{-0.05}$	$1.86^{+0.05}_{-0.05}$	$1.82^{+0.05}_{-0.05}$	$1.89^{+0.05}_{-0.05}$	>260	>195	>248	$0.73^{+0.27}_{-0.23}$	$0.56^{+0.20}_{-0.18}$	$0.78^{+0.23}_{-0.21}$
	60101002004	07605303	LW	<0.92	<0.22	<0.48	$1.89^{+0.08}_{-0.06}$	$1.81^{+0.03}_{-0.03}$	$1.88^{+0.05}_{-0.03}$	$1.82^{+0.06}_{-0.03}$	$1.89^{+0.04}_{-0.04}$	>367	>259	>324	$0.80^{+0.33}_{-0.25}$	$0.60^{+0.24}_{-0.18}$	$0.84^{+0.29}_{-0.21}$
Mrk 1044	60401005002	08240803	SW	<1.15	<0.20	<0.42	$2.50^{+0.10}_{-0.09}$	$2.42^{+0.04}_{-0.04}$	$2.48^{+0.06}_{-0.04}$	$2.41^{+0.05}_{-0.04}$	$2.46^{+0.07}_{-0.04}$	>126	>123	>146	$1.75^{+0.61}_{-0.50}$	$1.31^{+0.43}_{-0.37}$	$1.52^{+0.46}_{-0.39}$
	60401005002	08240805	SW	<0.78	<0.18	<0.31	$2.32^{+0.08}_{-0.08}$	$2.27^{+0.05}_{-0.06}$	$2.34^{+0.04}_{-0.05}$	$2.32^{+0.05}_{-0.07}$	$2.35^{+0.04}_{-0.07}$	>129	>129	>144	$0.83^{+0.62}_{-0.41}$	$1.01^{+0.46}_{-0.49}$	$1.06^{+0.63}_{-0.28}$
3C 109	60301011002	07956001	LW	<2.68	<2.63	<2.95	$1.68^{+0.12}_{-0.17}$	$1.69^{+0.18}_{-0.16}$	$1.79^{+0.18}_{-0.18}$	$1.76^{+0.14}_{-0.24}$	$1.85^{+0.10}_{-0.30}$	>67	>74	>85	<0.32	<0.55	<0.40
NGC 1566	80301601002	08008402	SW	$0.62^{+0.24}_{-0.49}$	<0.12	<0.35	$1.84^{+0.03}_{-0.05}$	$1.77^{+0.02}_{-0.02}$	$1.85^{+0.03}_{-0.02}$	$1.77^{+0.03}_{-0.02}$	$1.83^{+0.04}_{-0.02}$	>610	>351	>475	$0.74^{+0.16}_{-0.15}$	$0.60^{+0.12}_{-0.11}$	$0.79^{+0.15}_{-0.13}$
	80401601002	08205304	SW	<1.57	<0.37	<0.71	$1.77^{+0.08}_{-0.09}$	$1.60^{+0.04}_{-0.03}$	$1.69^{+0.06}_{-0.04}$	$1.69^{+0.06}_{-0.06}$	$1.73^{+0.06}_{-0.06}$	>241	>158	>182	$0.67^{+0.29}_{-0.25}$	$0.49^{+0.23}_{-0.20}$	$0.64^{+0.24}_{-0.22}$
	80502606002	08408004	SW	$1.51^{+1.04}_{-1.27}$	<0.31	<0.47	$1.78^{+0.04}_{-0.12}$	$1.62^{+0.04}_{-0.04}$	$1.69^{+0.04}_{-0.04}$	$1.65^{+0.08}_{-0.08}$	$1.70^{+0.08}_{-0.07}$	>182	>106	>117	$0.42^{+0.36}_{-0.28}$	$0.25^{+0.27}_{-0.23}$	$0.36^{+0.30}_{-0.25}$
1H 0419-577	60402006002	08203601	SW	<2.01	<0.59	<0.87	$1.65^{+0.14}_{-0.17}$	$1.55^{+0.05}_{-0.04}$	$1.62^{+0.05}_{-0.04}$	$1.52^{+0.11}_{-0.05}$	$1.59^{+0.10}_{-0.06}$	63^{+46}_{-24}	52^{+31}_{-13}	56^{+35}_{-18}	<0.55	<0.35	<0.53
	60402006004	08203602	SW	<2.15	<0.42	<0.56	$1.55^{+0.19}_{-0.13}$	$1.50^{+0.05}_{-0.05}$	$1.57^{+0.05}_{-0.05}$	$1.50^{+0.06}_{-0.06}$	$1.55^{+0.10}_{-0.06}$	54^{+58}_{-19}	49^{+21}_{-14}	50^{+35}_{-14}	<0.52	<0.40	<0.60
Ark 120	60001044002	06937815	SW	<0.74	$0.57^{+0.49}_{-0.49}$	$0.94^{+0.50}_{-0.49}$	$1.83^{+0.08}_{-0.04}$	$1.79^{+0.06}_{-0.06}$	$1.90^{+0.06}_{-0.06}$	$1.88^{+0.05}_{-0.05}$	$1.93^{+0.05}_{-0.05}$	>612	>714	>881	$0.49^{+0.27}_{-0.17}$	$0.54^{+0.22}_{-0.19}$	$0.77^{+0.26}_{-0.22}$
	60001044004	07216004	SW	<0.40	<0.13	<0.32	$1.98^{+0.05}_{-0.03}$	$1.90^{+0.02}_{-0.02}$	$1.97^{+0.02}_{-0.02}$	$1.92^{+0.04}_{-0.02}$	$1.98^{+0.02}_{-0.02}$	>346	>266	>335	$0.69^{+0.18}_{-0.18}$	$0.50^{+0.15}_{-0.07}$	$0.69^{+0.17}_{-0.15}$
ESO 362-18	60201046002	07908101	SW	<2.08	<0.36	<0.55	$1.48^{+0.14}_{-0.12}$	$1.33^{+0.04}_{-0.05}$	$1.40^{+0.06}_{-0.05}$	$1.42^{+0.08}_{-0.08}$	$1.46^{+0.08}_{-0.08}$	119^{+149}_{-45}	95^{+67}_{-28}	101^{+75}_{-31}	$0.56^{+0.39}_{-0.31}$	$0.42^{+0.29}_{-0.24}$	$0.57^{+0.32}_{-0.27}$
2MASX J05210136-2521450	60201022002	07905801	FF	$7.44^{+2.00}_{-2.04}$	$7.72^{+1.25}_{-1.23}$	$8.10^{+1.25}_{-1.23}$	$2.11^{+0.17}_{-0.17}$	$2.12^{+0.14}_{-0.14}$	$2.24^{+0.14}_{-0.14}$	$2.15^{+0.13}_{-0.13}$	$2.19^{+0.13}_{-0.12}$	>114	>103	>115	<0.87	<0.94	$0.57^{+0.66}_{-0.47}$
Mrk 79	60601010004	08708801	SW	<1.47	<0.74	<1.09	$1.77^{+0.16}_{-0.08}$	$1.77^{+0.05}_{-0.05}$	$1.86^{+0.11}_{-0.06}$	$1.77^{+0.06}_{-0.06}$	$1.83^{+0.06}_{-0.06}$	>64	121^{+575}_{-54}	>75	$0.62^{+0.61}_{-0.42}$	$0.61^{+0.50}_{-0.40}$	$0.80^{+0.55}_{-0.43}$
Mrk 110	60502022002	08525901	SW	<2.42	<0.75	<1.09	$1.87^{+0.13}_{-0.13}$	$1.70^{+0.05}_{-0.05}$	$1.78^{+0.11}_{-0.06}$	$1.80^{+0.08}_{-0.12}$	$1.85^{+0.07}_{-0.12}$	>114	>77	>94	<0.39	<0.19	<0.25
	60502022004	08525902	SW	$1.72^{+1.06}_{-1.05}$	<0.71	<1.08	$1.87^{+0.11}_{-0.11}$	$1.74^{+0.08}_{-0.04}$	$1.85^{+0.08}_{-0.07}$	$1.77^{+0.08}_{-0.08}$	$1.81^{+0.08}_{-0.08}$	>111	>86	>93	$0.38^{+0.37}_{-0.30}$	<0.52	$0.39^{+0.32}_{-0.27}$
NGC 2992	90501623002	08409203	SW	$0.94^{+0.42}_{-0.42}$	$0.89^{+0.24}_{-0.24}$	$1.26^{+0.24}_{-0.24}$	$1.67^{+0.04}_{-0.04}$	$1.56^{+0.03}_{-0.03}$	$1.67^{+0.03}_{-0.03}$	$1.67^{+0.03}_{-0.03}$	$1.71^{+0.03}_{-0.03}$	353^{+545}_{-134}	302^{+278}_{-99}	377^{+515}_{-138}	<0.16	<0.09	$0.13^{+0.08}_{-0.07}$
MCG -05-23-016	60701014002	08906701	SW	$1.61^{+0.47}_{-0.47}$	$1.75^{+0.30}_{-0.29}$	$2.15^{+0.29}_{-0.29}$	$1.83^{+0.05}_{-0.05}$	$1.80^{+0.03}_{-0.03}$	$1.91^{+0.03}_{-0.03}$	$1.83^{+0.04}_{-0.04}$	$1.89^{+0.04}_{-0.04}$	110^{+29}_{-19}	109^{+24}_{-17}	124^{+32}_{-21}	$0.77^{+0.17}_{-0.15}$	$0.72^{+0.14}_{-0.13}$	$0.96^{+0.17}_{-0.15}$
NGC 3227	60202002002	07825202	SW	$1.67^{+0.86}_{-0.86}$	$1.42^{+0.55}_{-0.55}$	$1.78^{+0.55}_{-0.55}$	$1.80^{+0.10}_{-0.10}$	$1.61^{+0.06}_{-0.06}$	$1.72^{+0.06}_{-0.06}$	$1.72^{+0.06}_{-0.06}$	$1.77^{+0.07}_{-0.06}$	189^{+260}_{-73}	147^{+104}_{-44}	171^{+147}_{-56}	$1.20^{+0.40}_{-0.33}$	$0.84^{+0.27}_{-0.23}$	$1.03^{+0.30}_{-0.26}$
	60202002004	07825203	SW	<1.87	$0.91^{+0.66}_{-0.65}$	$1.28^{+0.66}_{-0.65}$	$1.61^{+0.13}_{-0.11}$	$1.52^{+0.07}_{-0.07}$	$1.64^{+0.07}_{-0.07}$	$1.64^{+0.08}_{-0.07}$	$1.69^{+0.08}_{-0.08}$	98^{+64}_{-29}	104^{+57}_{-28}	115^{+69}_{-33}	$0.88^{+0.41}_{-0.33}$	$0.83^{+0.33}_{-0.27}$	$1.02^{+0.36}_{-0.30}$
	60202002006	07825204	SW	$1.51^{+0.75}_{-0.77}$	<0.79	$0.65^{+0.52}_{-0.51}$	$1.82^{+0.08}_{-0.08}$	$1.62^{+0.06}_{-0.05}$	$1.73^{+0.06}_{-0.06}$	$1.71^{+0.06}_{-0.06}$	$1.76^{+0.06}_{-0.06}$	>166	186^{+192}_{-65}	219^{+290}_{-83}	$0.94^{+0.32}_{-0.27}$	$0.66^{+0.23}_{-0.20}$	$0.83^{+0.26}_{-0.22}$
	60202002008	07825205	SW	$1.35^{+0.55}_{-0.65}$	<0.70	$0.62^{+0.48}_{-0.47}$	$1.86^{+0.05}_{-0.07}$	$1.69^{+0.05}_{-0.04}$	$1.80^{+0.05}_{-0.05}$	$1.77^{+0.05}_{-0.05}$	$1.81^{+0.05}_{-0.05}$	>510	>262	>330	$0.89^{+0.25}_{-0.23}$	$0.63^{+0.19}_{-0.17}$	$0.79^{+0.21}_{-0.19}$
	60202002010	07825206	SW	<0.94	<0.45	$0.44^{+0.38}_{-0.38}$	$1.81^{+0.07}_{-0.06}$	$1.70^{+0.04}_{-0.03}$	$1.81^{+0.04}_{-0.04}$	$1.75^{+0.05}_{-0.04}$	$1.83^{+0.05}_{-0.05}$	244^{+312}_{-89}	207^{+156}_{-64}	255^{+256}_{-88}	$0.94^{+0.26}_{-0.23}$	$0.79^{+0.20}_{-0.17}$	$0.99^{+0.22}_{-0.20}$
	60202002012	07825207	SW	$2.04^{+0.63}_{-0.73}$	$1.35^{+0.46}_{-0.46}$	$1.72^{+0.46}_{-0.46}$	$1.92^{+0.07}_{-0.08}$	$1.77^{+0.05}_{-0.05}$	$1.88^{+0.05}_{-0.05}$	$1.84^{+0.05}_{-0.05}$	$1.89^{+0.05}_{-0.05}$	>322	>234	>295	$1.06^{+0.33}_{-0.28}$	$0.79^{+0.23}_{-0.21}$	$0.98^{+0.26}_{-0.23}$
	80502609002	08443413	SW	$2.18^{+1.07}_{-1.06}$	$3.56^{+0.62}_{-0.61}$	$3.94^{+0.62}_{-0.61}$	$1.60^{+0.10}_{-0.10}$	$1.68^{+0.07}_{-0.07}$	$1.79^{+0.07}_{-0.07}$	$1.70^{+0.07}_{-0.07}$	$1.75^{+0.07}_{-0.07}$	167^{+319}_{-69}	>132	>149	$0.33^{+0.25}_{-0.21}$	$0.48^{+0.24}_{-0.21}$	$0.65^{+0.27}_{-0.23}$
	80502609004	08443414	SW	$4.42^{+2.39}_{-2.46}$	<2.43	$1.45^{+1.36}_{-1.34}$	$1.61^{+0.23}_{-0.23}$	$1.35^{+0.15}_{-0.14}$	$1.46^{+0.15}_{-0.14}$	$1.41^{+0.14}_{-0.14}$	$1.46^{+0.15}_{-0.14}$	>68	84^{+142}_{-34}	90^{+161}_{-37}	$0.68^{+0.77}_{-0.51}$	$0.45^{+0.54}_{-0.39}$	$0.61^{+0.61}_{-0.43}$
2MASSi J10315431-1416513	60701046002	08904101	SW	<1.11	<0.38	<0.60	$1.79^{+0.13}_{-0.07}$	$1.75^{+0.04}_{-0.04}$	$1.82^{+0.07}_{-0.04}$	$1.76^{+0.07}_{-0.05}$	$1.82^{+0.05}_{-0.05}$	153^{+412}_{-62}	143^{+229}_{-54}	169^{+340}_{-70}	$0.70^{+0.41}_{-0.33}$	$0.55^{+0.31}_{-0.26}$	$0.74^{+0.35}_{-0.29}$
NGC 3516	60160001002	08545911	SW	<2.37	$1.63^{+1.00}_{-0.99}$	$2.00^{+1.00}_{-0.99}$	$1.70^{+0.19}_{-0.15}$	$1.69^{+0.11}_{-0.11}$	$1.80^{+0.11}_{-0.11}$	$1.78^{+0.12}_{-0.11}$	$1.83^{+0.12}_{-0.12}$	>90	>106	>117	$0.77^{+0.69}_{-0.50}$	$0.86^{+0.58}_{-0.44}$	$1.09^{+0.66}_{-0.50}$
HE 1136-2304	80002031002	07412601	SW	<2.91	<1.75	$1.15^{+0.96}_{-0.95}$	$1.78^{+0.16}_{-0.16}$	$1.65^{+0.11}_{-0.11}$	$1.76^{+0.11}_{-0.11}$	$1.73^{+0.11}_{-0.11}$	$1.77^{+0.11}_{-0.11}$	>85	>78	>84	<0.79	<0.54	<0.72
	80002031003	07412601	SW	<1.65	<0.48	<0.62	$1.60^{+0.09}_{-0.09}$	$1.51^{+0.06}_{-0.06}$	$1.58^{+0.06}_{-0.06}$	$1.54^{+0.07}_{-0.07}$	$1.59^{+0.07}_{-0.07}$	110^{+376}_{-55}	85^{+91}_{-35}	100^{+269}_{-47}	<0.50	<0.34	<0.48

(To be continued on the next page)

DOI: 10.52396/JUSTC-2023-0160
JUSTC, **2024**, 54(7): 0702

(Continued)

Source	Nu ID	XMM ID	Mode	$N_{\rm H}^{\rm Nu}$ $10^{22}{\rm cm}^{-2}$	$N_{\rm H}^{\rm pn}$ $10^{22}{\rm cm}^{-2}$	$N_{\rm H}^{\rm pn-Cor}$ $10^{22}{\rm cm}^{-2}$	$\Gamma^{\rm Nu}$	$\Gamma^{\rm pn}$	$\Gamma^{\rm pn-Cor}$	$\Gamma^{\rm joint}$	$\Gamma^{\rm joint-Cor}$	$E_{\rm cut}^{\rm Nu}$ (keV)	$E_{\rm cut}^{\rm joint}$ (keV)	$E_{\rm cut}^{\rm joint-Cor}$ (keV)	$R^{\rm Nu}$	$R^{\rm joint}$	$R^{\rm joint-Cor}$
KUG 1141+371	90601618002	08711901001	SW	<3.63	<0.83	<1.02	$1.79^{+0.33}_{-0.23}$	$1.70^{+0.08}_{-0.08}$	$1.77^{+0.13}_{-0.08}$	$1.67^{+0.17}_{-0.11}$	$1.73^{+0.11}_{-0.11}$	40^{+102}_{-17}	39^{+67}_{-14}	43^{+71}_{-16}	$0.94^{+1.50}_{-0.88}$	<1.39	<1.59
2MASX J11454045-1827149	60302002002	07955801001	SW	<2.07	<0.91	<1.28	$1.74^{+0.15}_{-0.14}$	$1.63^{+0.10}_{-0.05}$	$1.74^{+0.10}_{-0.08}$	$1.67^{+0.10}_{-0.10}$	$1.71^{+0.10}_{-0.09}$	64^{+62}_{-22}	58^{+44}_{-18}	61^{+49}_{-19}	$0.51^{+0.51}_{-0.39}$	$0.32^{+0.38}_{-0.31}$	$0.46^{+0.42}_{-0.34}$
	60302002004	07955802001	SW	<1.60	<0.43	<0.54	$1.67^{+0.18}_{-0.09}$	$1.54^{+0.06}_{-0.06}$	$1.61^{+0.06}_{-0.06}$	$1.59^{+0.12}_{-0.07}$	$1.63^{+0.07}_{-0.07}$	>54	95^{+253}_{-42}	111^{+367}_{-53}	<0.84	<0.34	<0.45
	60302002006	07955803001	SW	<1.71	<0.39	<0.58	$1.75^{+0.16}_{-0.08}$	$1.70^{+0.04}_{-0.04}$	$1.77^{+0.04}_{-0.04}$	$1.71^{+0.07}_{-0.05}$	$1.76^{+0.05}_{-0.05}$	126^{+593}_{-53}	121^{+239}_{-48}	138^{+357}_{-58}	<0.64	<0.41	$0.26^{+0.30}_{-0.25}$
	60302002008	07955804001	SW	$1.63^{+1.31}_{-1.38}$	<0.74	<1.10	$1.89^{+0.14}_{-0.15}$	$1.72^{+0.04}_{-0.04}$	$1.82^{+0.10}_{-0.07}$	$1.77^{+0.10}_{-0.10}$	$1.81^{+0.10}_{-0.10}$	>91	>69	>74	$0.43^{+0.50}_{-0.39}$	<0.64	$0.41^{+0.42}_{-0.34}$
	60302002010	07955805001	SW	<2.84	<0.48	<0.70	$1.90^{+0.15}_{-0.19}$	$1.73^{+0.05}_{-0.05}$	$1.79^{+0.10}_{-0.03}$	$1.71^{+0.10}_{-0.06}$	$1.76^{+0.10}_{-0.06}$	>78	>67	>69	$0.50^{+0.56}_{-0.49}$	<0.54	<0.75
NGC 4051	60401009002	08304302001	SW	<1.30	<0.36	<0.59	$1.97^{+0.09}_{-0.09}$	$1.86^{+0.05}_{-0.04}$	$1.94^{+0.07}_{-0.04}$	$1.91^{+0.07}_{-0.07}$	$1.94^{+0.07}_{-0.06}$	>791	>446	>588	$1.67^{+0.60}_{-0.48}$	$1.36^{+0.48}_{-0.39}$	$1.61^{+0.53}_{-0.41}$
NGC 4593	60001149002	07409202001	SW	<1.80	<0.81	<1.11	$1.87^{+0.18}_{-0.13}$	$1.75^{+0.10}_{-0.06}$	$1.82^{+0.13}_{-0.06}$	$1.79^{+0.14}_{-0.10}$	$1.84^{+0.13}_{-0.09}$	>132	>105	>115	$0.88^{+0.92}_{-0.54}$	$0.64^{+0.67}_{-0.44}$	$0.83^{+0.75}_{-0.47}$
	60001149004	07409203001	SW	<3.92	<2.09	<2.47	$1.73^{+0.25}_{-0.20}$	$1.53^{+0.23}_{-0.05}$	$1.64^{+0.23}_{-0.14}$	$1.70^{+0.19}_{-0.17}$	$1.74^{+0.19}_{-0.17}$	>142	>119	>129	<1.42	<1.07	<1.30
	60001149006	07409204001	SW	<0.92	<1.62	<2.00	$1.79^{+0.12}_{-0.11}$	$1.62^{+0.06}_{-0.06}$	$1.69^{+0.06}_{-0.06}$	$1.67^{+0.08}_{-0.07}$	$1.73^{+0.09}_{-0.08}$	>204	>98	>114	$1.18^{+0.89}_{-0.56}$	$0.79^{+0.64}_{-0.47}$	$1.00^{+0.73}_{-0.51}$
	60001149008	07409205001	SW	<0.56	$1.90^{+1.07}_{-1.06}$	$2.28^{+1.07}_{-1.06}$	$1.85^{+0.09}_{-0.08}$	$1.71^{+0.07}_{-0.06}$	$1.78^{+0.07}_{-0.06}$	$1.77^{+0.06}_{-0.06}$	$1.81^{+0.06}_{-0.06}$	>612	>489	>545	$0.67^{+0.49}_{-0.35}$	$0.37^{+0.32}_{-0.25}$	$0.51^{+0.35}_{-0.27}$
	60001149010	07409206001	SW	<1.58	<0.42	<0.59	$1.83^{+0.12}_{-0.10}$	$1.71^{+0.05}_{-0.06}$	$1.78^{+0.07}_{-0.05}$	$1.75^{+0.09}_{-0.07}$	$1.79^{+0.08}_{-0.06}$	>165	>127	>147	$0.40^{+0.46}_{-0.31}$	<0.59	$0.36^{+0.39}_{-0.26}$
MCG -06-30-015	60001047003	06937812001	SW	$1.79^{+0.39}_{-0.45}$	$1.25^{+0.32}_{-0.32}$	$1.62^{+0.32}_{-0.32}$	$2.33^{+0.05}_{-0.06}$	$2.26^{+0.04}_{-0.04}$	$2.37^{+0.04}_{-0.04}$	$2.27^{+0.04}_{-0.04}$	$2.33^{+0.04}_{-0.04}$	>576	>356	>635	$1.71^{+0.35}_{-0.30}$	$1.43^{+0.26}_{-0.23}$	$1.77^{+0.27}_{-0.27}$
	60001047003	06937813001	SW	$1.84^{+0.40}_{-0.43}$	$1.09^{+0.34}_{-0.34}$	$1.47^{+0.34}_{-0.34}$	$2.24^{+0.05}_{-0.05}$	$2.10^{+0.04}_{-0.04}$	$2.21^{+0.04}_{-0.04}$	$2.16^{+0.05}_{-0.04}$	$2.24^{+0.02}_{-0.05}$	>693	>318	>503	$1.75^{+0.35}_{-0.31}$	$1.41^{+0.26}_{-0.23}$	$1.80^{+0.32}_{-0.26}$
	60001047005	06937814001	SW	$1.40^{+0.90}_{-1.02}$	$1.54^{+0.78}_{-0.78}$	$1.91^{+0.78}_{-0.78}$	$2.12^{+0.11}_{-0.12}$	$2.07^{+0.10}_{-0.09}$	$2.18^{+0.10}_{-0.09}$	$2.11^{+0.09}_{-0.09}$	$2.15^{+0.09}_{-0.09}$	>281	>326	>425	$1.87^{+0.88}_{-0.66}$	$1.74^{+0.69}_{-0.53}$	$2.06^{+0.78}_{-0.60}$
IC 4329A	60702050002	08620901001	SW	$1.04^{+0.98}_{-1.02}$	$0.78^{+0.57}_{-0.57}$	$1.15^{+0.57}_{-0.57}$	$1.82^{+0.10}_{-0.11}$	$1.75^{+0.07}_{-0.07}$	$1.86^{+0.07}_{-0.07}$	$1.81^{+0.07}_{-0.07}$	$1.86^{+0.07}_{-0.07}$	>138	>142	>164	$0.58^{+0.33}_{-0.27}$	$0.51^{+0.26}_{-0.23}$	$0.68^{+0.30}_{-0.25}$
	60702050004	08620903001	SW	<2.11	<1.21	$0.86^{+0.72}_{-0.71}$	$1.74^{+0.11}_{-0.12}$	$1.67^{+0.08}_{-0.08}$	$1.78^{+0.08}_{-0.08}$	$1.71^{+0.04}_{-0.08}$	$1.75^{+0.04}_{-0.07}$	>227	>204	>237	<0.54	<0.39	$0.28^{+0.27}_{-0.20}$
	60702050006	08620905001	SW	<1.39	<1.00	$0.87^{+0.52}_{-0.51}$	$1.79^{+0.07}_{-0.07}$	$1.74^{+0.06}_{-0.06}$	$1.85^{+0.06}_{-0.06}$	$1.77^{+0.05}_{-0.05}$	$1.81^{+0.05}_{-0.05}$	>450	>398	>530	$0.26^{+0.20}_{-0.17}$	$0.21^{+0.16}_{-0.14}$	$0.36^{+0.18}_{-0.16}$
	60702050010	08620909001	SW	<4.75	<0.71	<1.77	$1.79^{+0.34}_{-0.28}$	$1.58^{+0.17}_{-0.10}$	$1.66^{+0.20}_{-0.10}$	$1.66^{+0.22}_{-0.20}$	$1.70^{+0.21}_{-0.19}$	>24	>24	>25	<2.46	<1.33	<1.60
NGC 5548	60002044003	07201106001	SW	$2.67^{+0.73}_{-0.78}$	$2.83^{+0.49}_{-0.49}$	$3.20^{+0.49}_{-0.49}$	$1.77^{+0.08}_{-0.08}$	$1.65^{+0.06}_{-0.05}$	$1.76^{+0.06}_{-0.05}$	$1.73^{+0.05}_{-0.05}$	$1.78^{+0.05}_{-0.05}$	>186	>177	>214	$0.64^{+0.26}_{-0.22}$	$0.45^{+0.19}_{-0.17}$	$0.61^{+0.21}_{-0.19}$
	60002044005	07201110001	SW	$2.94^{+0.64}_{-0.87}$	$3.78^{+0.56}_{-0.56}$	$4.16^{+0.56}_{-0.56}$	$1.52^{+0.09}_{-0.09}$	$1.53^{+0.06}_{-0.06}$	$1.64^{+0.06}_{-0.06}$	$1.57^{+0.06}_{-0.06}$	$1.62^{+0.06}_{-0.06}$	94^{+39}_{-23}	102^{+42}_{-23}	113^{+51}_{-28}	$0.46^{+0.22}_{-0.20}$	$0.52^{+0.21}_{-0.18}$	$0.69^{+0.23}_{-0.20}$
	60002044008	07201115001	SW	$3.24^{+1.07}_{-1.09}$	$3.57^{+0.66}_{-0.66}$	$3.94^{+0.66}_{-0.66}$	$1.50^{+0.10}_{-0.11}$	$1.45^{+0.07}_{-0.07}$	$1.56^{+0.07}_{-0.07}$	$1.50^{+0.07}_{-0.07}$	$1.55^{+0.07}_{-0.07}$	107^{+68}_{-31}	108^{+55}_{-28}	119^{+67}_{-32}	$0.38^{+0.24}_{-0.21}$	$0.34^{+0.20}_{-0.17}$	$0.46^{+0.21}_{-0.19}$
ESO 511-G030	60502035002	08520101001	SW	<4.68	<1.08	<1.46	$1.72^{+0.33}_{-0.26}$	$1.56^{+0.17}_{-0.10}$	$1.60^{+0.18}_{-0.10}$	$1.61^{+0.14}_{-0.17}$	$1.61^{+0.12}_{-0.12}$	>40	>42	>44	<1.51	<0.70	<0.80
	60502035004	08520102001	SW	<5.03	<1.61	<1.93	$1.73^{+0.24}_{-0.22}$	$1.51^{+0.19}_{-0.10}$	$1.58^{+0.23}_{-0.09}$	$1.64^{+0.14}_{-0.23}$	$1.64^{+0.16}_{-0.18}$	>82	>54	>60	<0.37	<0.45	<0.52
	60502035006	08520103001	SW	<3.50	<0.69	<0.79	$1.45^{+0.15}_{-0.17}$	$1.47^{+0.11}_{-0.10}$	$1.54^{+0.10}_{-0.09}$	$1.43^{+0.12}_{-0.12}$	$1.55^{+0.09}_{-0.21}$	>30	52^{+82}_{-21}	66^{+199}_{-30}	<0.76	<0.50	<0.58
	60502035008	08520104001	SW	<2.42	<0.87	<1.03	$1.57^{+0.16}_{-0.16}$	$1.54^{+0.10}_{-0.10}$	$1.61^{+0.10}_{-0.10}$	$1.55^{+0.12}_{-0.12}$	$1.61^{+0.12}_{-0.12}$	>35	>34	>36	<1.23	<1.19	<1.43
Mrk 1383	60501049002	08522101001	SW	<0.85	<2.07	$1.28^{+1.14}_{-1.15}$	$1.77^{+0.10}_{-0.10}$	$1.77^{+0.06}_{-0.06}$	$1.84^{+0.06}_{-0.06}$	$1.77^{+0.07}_{-0.07}$	$1.83^{+0.08}_{-0.07}$	>84	>80	>89	$0.55^{+0.63}_{-0.42}$	$0.57^{+0.56}_{-0.42}$	$0.78^{+0.63}_{-0.46}$
Mrk 817	60702008002	08823406001	LW	$1.98^{+0.56}_{-0.71}$	$2.49^{+0.55}_{-0.52}$	$2.79^{+0.59}_{-0.46}$	$2.16^{+0.09}_{-0.08}$	$2.15^{+0.07}_{-0.06}$	$2.26^{+0.08}_{-0.06}$	$2.15^{+0.06}_{-0.06}$	$2.19^{+0.06}_{-0.06}$	>988	>1112	>1310	$1.57^{+0.54}_{-0.44}$	$1.36^{+0.38}_{-0.33}$	$1.64^{+0.42}_{-0.36}$
	60702008004	08823407001	LW	$4.87^{+1.53}_{-1.54}$	$6.98^{+0.91}_{-0.91}$	$7.36^{+0.91}_{-0.91}$	$1.70^{+0.16}_{-0.16}$	$1.77^{+0.10}_{-0.10}$	$1.88^{+0.10}_{-0.10}$	$1.77^{+0.10}_{-0.10}$	$1.83^{+0.10}_{-0.10}$	114^{+244}_{-49}	162^{+704}_{-77}	>95	$0.95^{+0.60}_{-0.45}$	$0.92^{+0.47}_{-0.38}$	$1.16^{+0.53}_{-0.42}$
	60702008006	08823408001	LW	$2.79^{+1.24}_{-1.61}$	$5.12^{+0.95}_{-0.94}$	$5.50^{+0.96}_{-0.94}$	$1.89^{+0.12}_{-0.18}$	$1.99^{+0.11}_{-0.11}$	$2.10^{+0.11}_{-0.11}$	$1.95^{+0.10}_{-0.09}$	$1.99^{+0.10}_{-0.09}$	>168	>395	>497	$1.65^{+0.91}_{-0.42}$	$1.74^{+0.73}_{-0.56}$	$2.05^{+0.81}_{-0.62}$
Mrk 841	60101023002	07637905001	FF	<2.49	<2.04	$1.21^{+1.20}_{-1.18}$	$1.88^{+0.28}_{-0.13}$	$1.94^{+0.15}_{-0.13}$	$2.06^{+0.15}_{-0.14}$	$1.95^{+0.16}_{-0.16}$	$2.01^{+0.08}_{-0.15}$	>62	>73	>84	$0.99^{+1.28}_{-0.70}$	$1.02^{+0.93}_{-0.65}$	$1.27^{+1.04}_{-0.71}$
	60702007002	08821303001	SW	<1.67	<0.64	<1.02	$1.85^{+0.14}_{-0.11}$	$1.80^{+0.07}_{-0.04}$	$1.91^{+0.07}_{-0.07}$	$1.81^{+0.08}_{-0.06}$	$1.88^{+0.09}_{-0.07}$	>95	145^{+227}_{-57}	168^{+341}_{-71}	$0.95^{+0.51}_{-0.41}$	$0.90^{+0.40}_{-0.33}$	$1.20^{+0.48}_{-0.38}$
	60702007002	08821304001	SW	<1.39	<0.42	<0.72	$1.90^{+0.10}_{-0.09}$	$1.82^{+0.05}_{-0.04}$	$1.90^{+0.08}_{-0.04}$	$1.85^{+0.07}_{-0.07}$	$1.89^{+0.07}_{-0.05}$	>395	>295	>354	$0.66^{+0.39}_{-0.31}$	$0.50^{+0.29}_{-0.23}$	$0.67^{+0.32}_{-0.24}$
	80701616002	08906402001	SW	<2.01	<0.63	<0.99	$1.87^{+0.18}_{-0.13}$	$1.75^{+0.04}_{-0.04}$	$1.84^{+0.09}_{-0.06}$	$1.78^{+0.11}_{-0.08}$	$1.84^{+0.11}_{-0.08}$	107^{+264}_{-46}	91^{+121}_{-34}	99^{+147}_{-38}	$1.19^{+0.79}_{-0.57}$	$0.84^{+0.53}_{-0.42}$	$1.10^{+0.61}_{-0.47}$
3C 382	60202015002	07906001001	SW	<1.19	<1.13	<1.50	$1.76^{+0.05}_{-0.08}$	$1.72^{+0.10}_{-0.07}$	$1.83^{+0.10}_{-0.10}$	$1.75^{+0.05}_{-0.09}$	$1.77^{+0.04}_{-0.07}$	>140	>118	>179	<0.25	<0.24	<0.38

(To be continued on the next page)

DOI: 10.52396/JUSTC-2023-0160
JUSTC, **2024**, 54(7): 0702

(Continued)

Source	Nu ID	XMM ID	Mode	$N_{\rm H}^{\rm Nu}$ $10^{22}{\rm cm}^{-2}$	$N_{\rm H}^{\rm pn}$ $10^{22}{\rm cm}^{-2}$	$N_{\rm H}^{\rm pn-Cor}$ $10^{22}{\rm cm}^{-2}$	$\Gamma^{\rm Nu}$	$\Gamma^{\rm pn}$	$\Gamma^{\rm pn-Cor}$	$\Gamma^{\rm joint}$	$\Gamma^{\rm joint-Cor}$	$E_{\rm cut}^{\rm Nu}$ (keV)	$E_{\rm cut}^{\rm joint}$ (keV)	$E_{\rm cut}^{\rm joint-Cor}$ (keV)	$R^{\rm Nu}$	$R^{\rm joint}$	$R^{\rm joint-Cor}$
	60202015004	07906002 01	SW	<1.47	<1.07	$0.73^{+0.71}_{-0.71}$	$1.70^{+0.12}_{-0.09}$	$1.61^{+0.08}_{-0.07}$	$1.72^{+0.08}_{-0.08}$	$1.68^{+0.08}_{-0.08}$	$1.72^{+0.08}_{-0.08}$	76^{+62}_{-23}	73^{+50}_{-21}	79^{+58}_{-24}	<0.58	<0.43	$0.30^{+0.29}_{-0.24}$
	60202015006	07906003 01	SW	<0.82	<1.70	$1.19^{+0.89}_{-0.91}$	$1.74^{+0.07}_{-0.06}$	$1.59^{+0.08}_{-0.05}$	$1.68^{+0.07}_{-0.07}$	$1.66^{+0.05}_{-0.06}$	$1.69^{+0.05}_{-0.05}$	>120	144^{+373}_{-63}	>98	<0.27	<0.16	<0.18
	60202015008	07906004 01	SW	<2.55	<0.34	<0.50	$1.76^{+0.15}_{-0.14}$	$1.66^{+0.05}_{-0.04}$	$1.73^{+0.04}_{-0.04}$	$1.66^{+0.04}_{-0.05}$	$1.70^{+0.08}_{-0.04}$	>86	133^{+152}_{-47}	190^{+541}_{-93}	<0.37	<0.15	<0.27
	60202015010	07906005 01	SW	<1.02	<0.57	<0.90	$1.77^{+0.05}_{-0.06}$	$1.60^{+0.04}_{-0.04}$	$1.67^{+0.04}_{-0.04}$	$1.67^{+0.05}_{-0.05}$	$1.71^{+0.05}_{-0.06}$	>138	140^{+278}_{-57}	>97	<0.26	<0.11	<0.14
Fairall 49	60301028002	07956901 01	SW	$2.01^{+1.00}_{-1.06}$	$1.66^{+0.63}_{-0.63}$	$2.06^{+0.63}_{-0.63}$	$2.49^{+0.12}_{-0.13}$	$2.33^{+0.08}_{-0.08}$	$2.44^{+0.08}_{-0.08}$	$2.42^{+0.09}_{-0.09}$	$2.47^{+0.09}_{-0.09}$	>116	>110	>129	$1.43^{+0.74}_{-0.57}$	$1.05^{+0.52}_{-0.43}$	$1.26^{+0.57}_{-0.46}$
2MASX J19373299-0613046	60101003002	07618702 01	SW	<1.22	<0.13	<0.26	$2.42^{+0.16}_{-0.10}$	$2.24^{+0.04}_{-0.03}$	$2.31^{+0.04}_{-0.03}$	$2.28^{+0.08}_{-0.06}$	$2.33^{+0.08}_{-0.06}$	>129	180^{+552}_{-79}	>115	$1.83^{+0.74}_{-0.61}$	$1.16^{+0.57}_{-0.39}$	$1.31^{+0.56}_{-0.40}$
	60702018004	08910101 01	SW	$0.97^{+0.68}_{-0.75}$	$0.63^{+0.48}_{-0.47}$	$1.01^{+0.48}_{-0.47}$	$2.45^{+0.11}_{-0.10}$	$2.33^{+0.07}_{-0.07}$	$2.44^{+0.07}_{-0.07}$	$2.42^{+0.10}_{-0.08}$	$2.46^{+0.10}_{-0.08}$	>220	>202	>264	$1.52^{+0.85}_{-0.55}$	$1.32^{+0.80}_{-0.49}$	$1.56^{+0.89}_{-0.52}$
	60702018004	08910102 01	SW	<0.92	<0.79	$0.72^{+0.48}_{-0.48}$	$2.30^{+0.09}_{-0.07}$	$2.28^{+0.07}_{-0.06}$	$2.40^{+0.07}_{-0.07}$	$2.35^{+0.07}_{-0.07}$	$2.40^{+0.07}_{-0.07}$	>125	>120	>140	$0.78^{+0.43}_{-0.34}$	$1.15^{+0.42}_{-0.37}$	$1.37^{+0.45}_{-0.43}$
NGC 6814	60701012002	08850901 01	LW	<1.24	<0.17	<0.40	$1.83^{+0.07}_{-0.07}$	$1.74^{+0.02}_{-0.02}$	$1.80^{+0.04}_{-0.02}$	$1.76^{+0.04}_{-0.04}$	$1.82^{+0.04}_{-0.04}$	>484	>274	>353	$0.46^{+0.24}_{-0.20}$	$0.28^{+0.17}_{-0.15}$	$0.46^{+0.19}_{-0.16}$
SWIFT J212745.6+565636	60001110002	06937817 01	SW	<0.57	<0.66	$0.55^{+0.48}_{-0.48}$	$1.87^{+0.08}_{-0.05}$	$1.82^{+0.06}_{-0.04}$	$1.93^{+0.06}_{-0.06}$	$1.84^{+0.07}_{-0.06}$	$1.91^{+0.07}_{-0.07}$	66^{+20}_{-12}	64^{+20}_{-13}	70^{+24}_{-15}	$1.39^{+0.46}_{-0.35}$	$1.18^{+0.36}_{-0.31}$	$1.50^{+0.43}_{-0.36}$
	60001110003	06937817 01	SW	<1.67	<1.17	$0.95^{+0.59}_{-0.58}$	$1.94^{+0.12}_{-0.12}$	$1.89^{+0.07}_{-0.07}$	$2.00^{+0.07}_{-0.07}$	$1.92^{+0.08}_{-0.08}$	$1.98^{+0.08}_{-0.08}$	92^{+64}_{-28}	87^{+45}_{-23}	98^{+59}_{-28}	$1.43^{+0.56}_{-0.45}$	$1.36^{+0.44}_{-0.37}$	$1.65^{+0.49}_{-0.41}$
	60001110005	06937818 01	SW	$1.18^{+0.58}_{-0.59}$	<0.62	$0.64^{+0.35}_{-0.35}$	$2.00^{+0.07}_{-0.07}$	$1.88^{+0.04}_{-0.04}$	$1.99^{+0.04}_{-0.04}$	$1.91^{+0.05}_{-0.05}$	$1.98^{+0.05}_{-0.05}$	87^{+27}_{-17}	73^{+15}_{-11}	82^{+19}_{-13}	$1.73^{+0.36}_{-0.32}$	$1.47^{+0.27}_{-0.24}$	$1.80^{+0.31}_{-0.28}$
	60001110007	06937819 01	SW	<0.92	<0.72	$0.66^{+0.43}_{-0.43}$	$1.96^{+0.09}_{-0.08}$	$1.90^{+0.05}_{-0.05}$	$2.01^{+0.05}_{-0.05}$	$1.92^{+0.06}_{-0.06}$	$1.99^{+0.06}_{-0.06}$	59^{+16}_{-10}	54^{+11}_{-8}	59^{+14}_{-9}	$1.71^{+0.44}_{-0.38}$	$1.57^{+0.38}_{-0.34}$	$1.92^{+0.42}_{-0.36}$
2MASX J21344509-2725557	60363005002	08022002 01	LW	<2.09	<1.53	<1.94	$1.87^{+0.24}_{-0.18}$	$1.77^{+0.19}_{-0.08}$	$1.84^{+0.08}_{-0.08}$	$1.78^{+0.12}_{-0.11}$	$1.86^{+0.23}_{-0.13}$	>46	>40	>45	$0.75^{+1.30}_{-0.74}$	<1.54	$0.80^{+1.20}_{-0.71}$
NGC 7314	60201031002	07906501 01	SW	$0.81^{+0.78}_{-0.78}$	$0.74^{+0.47}_{-0.47}$	$1.11^{+0.47}_{-0.47}$	$2.01^{+0.09}_{-0.09}$	$1.93^{+0.06}_{-0.06}$	$2.04^{+0.06}_{-0.06}$	$1.99^{+0.06}_{-0.06}$	$2.04^{+0.06}_{-0.06}$	184^{+321}_{-74}	165^{+180}_{-58}	200^{+308}_{-78}	$1.00^{+0.36}_{-0.30}$	$0.90^{+0.32}_{-0.26}$	$1.09^{+0.34}_{-0.28}$
Mrk 915	60002060002	07444904 01	LW	$2.84^{+1.23}_{-1.24}$	$2.54^{+0.84}_{-0.83}$	$2.91^{+0.84}_{-0.83}$	$1.75^{+0.09}_{-0.11}$	$1.66^{+0.09}_{-0.09}$	$1.77^{+0.09}_{-0.09}$	$1.73^{+0.08}_{-0.08}$	$1.77^{+0.08}_{-0.08}$	>363	>290	>322	<0.61	<0.43	$0.32^{+0.31}_{-0.24}$
	60002060004	07444905 01	LW	<4.37	$2.62^{+1.45}_{-1.43}$	$3.00^{+1.46}_{-1.43}$	$1.40^{+0.24}_{-0.23}$	$1.41^{+0.16}_{-0.16}$	$1.52^{+0.16}_{-0.16}$	$1.44^{+0.16}_{-0.17}$	$1.48^{+0.16}_{-0.17}$	>33	74^{+434}_{-36}	>44	<0.41	<0.42	<0.58
	60002060006	07444906 01	LW	<8.91	<3.76	<4.14	$1.75^{+0.48}_{-0.48}$	$1.55^{+0.27}_{-0.23}$	$1.67^{+0.27}_{-0.25}$	$1.59^{+0.27}_{-0.28}$	$1.65^{+0.28}_{-0.28}$	>40	>39	>42	<3.43	<1.77	<2.17
MR 2251-178	60102025002	07639205 01	SW	<1.72	<1.75	$1.09^{+1.02}_{-1.01}$	$1.68^{+0.12}_{-0.10}$	$1.59^{+0.14}_{-0.16}$	$1.70^{+0.12}_{-0.12}$	$1.68^{+0.11}_{-0.12}$	$1.72^{+0.09}_{-0.12}$	>74	>66	>75	<0.10	<0.08	<0.10
	60102025004	07639206 01	SW	$1.09^{+0.96}_{-0.96}$	<1.08	$0.84^{+0.61}_{-0.61}$	$1.75^{+0.11}_{-0.11}$	$1.63^{+0.07}_{-0.07}$	$1.74^{+0.07}_{-0.07}$	$1.69^{+0.07}_{-0.07}$	$1.73^{+0.07}_{-0.07}$	117^{+146}_{-43}	100^{+66}_{-32}	111^{+106}_{-37}	<0.46	<0.25	<0.39
	60102025006	07639207 01	SW	$2.11^{+0.99}_{-0.99}$	<0.74	<1.21	$1.86^{+0.11}_{-0.11}$	$1.66^{+0.08}_{-0.04}$	$1.77^{+0.08}_{-0.08}$	$1.73^{+0.08}_{-0.08}$	$1.75^{+0.09}_{-0.09}$	>95	111^{+199}_{-44}	123^{+262}_{-50}	$0.30^{+0.34}_{-0.28}$	<0.50	$0.25^{+0.30}_{-0.25}$
	60102025008	07639208 01	SW	$1.66^{+1.31}_{-1.50}$	<1.13	<1.51	$1.85^{+0.14}_{-0.16}$	$1.63^{+0.08}_{-0.07}$	$1.74^{+0.08}_{-0.08}$	$1.70^{+0.09}_{-0.09}$	$1.76^{+0.09}_{-0.09}$	>78	114^{+132}_{-47}	130^{+412}_{-56}	$0.32^{+0.37}_{-0.31}$	<0.28	<0.42
	90601637002	08723908 01	SW	<2.08	$1.79^{+0.92}_{-0.91}$	$2.16^{+0.92}_{-0.91}$	$1.58^{+0.14}_{-0.13}$	$1.56^{+0.11}_{-0.11}$	$1.68^{+0.11}_{-0.11}$	$1.60^{+0.10}_{-0.11}$	$1.66^{+0.10}_{-0.10}$	67^{+66}_{-23}	74^{+78}_{-26}	79^{+90}_{-28}	<0.51	<0.43	<0.58
NGC 7469	60101001002	07603502 01	SW	<1.30	<0.36	<0.65	$1.92^{+0.12}_{-0.07}$	$1.83^{+0.03}_{-0.03}$	$1.91^{+0.07}_{-0.04}$	$1.89^{+0.07}_{-0.07}$	$1.94^{+0.07}_{-0.07}$	>125	>109	>125	$0.67^{+0.39}_{-0.30}$	$0.57^{+0.30}_{-0.26}$	$0.74^{+0.34}_{-0.28}$
	60101001004	07603503 01	SW	<1.13	<0.52	<0.88	$1.87^{+0.09}_{-0.08}$	$1.80^{+0.07}_{-0.03}$	$1.90^{+0.07}_{-0.06}$	$1.84^{+0.07}_{-0.06}$	$1.89^{+0.07}_{-0.06}$	>239	>171	>200	$0.48^{+0.36}_{-0.26}$	$0.47^{+0.31}_{-0.26}$	$0.67^{+0.36}_{-0.28}$
	60101001006	07603504 01	SW	<0.60	<0.51	<0.57	$1.89^{+0.07}_{-0.06}$	$1.77^{+0.04}_{-0.04}$	$1.84^{+0.04}_{-0.04}$	$1.81^{+0.05}_{-0.04}$	$1.86^{+0.05}_{-0.05}$	>274	>170	>210	$0.72^{+0.42}_{-0.30}$	$0.45^{+0.34}_{-0.15}$	$0.62^{+0.37}_{-0.16}$
	60101001010	07603506 01	SW	<0.70	<1.17	<1.50	$1.79^{+0.07}_{-0.07}$	$1.74^{+0.05}_{-0.05}$	$1.81^{+0.05}_{-0.05}$	$1.75^{+0.05}_{-0.05}$	$1.80^{+0.05}_{-0.05}$	>168	>153	>179	$0.32^{+0.40}_{-0.26}$	<0.51	$0.33^{+0.35}_{-0.22}$
	60101001012	07603507 01	SW	<0.55	<0.55	<0.80	$1.89^{+0.09}_{-0.08}$	$1.78^{+0.05}_{-0.05}$	$1.85^{+0.05}_{-0.05}$	$1.81^{+0.06}_{-0.05}$	$1.87^{+0.06}_{-0.06}$	>463	>306	>386	$0.96^{+0.55}_{-0.40}$	$0.64^{+0.36}_{-0.27}$	$0.88^{+0.41}_{-0.32}$
	60101001014	07603508 01	SW	<0.46	<0.30	<0.46	$1.86^{+0.06}_{-0.06}$	$1.74^{+0.04}_{-0.04}$	$1.82^{+0.04}_{-0.04}$	$1.80^{+0.04}_{-0.04}$	$1.85^{+0.04}_{-0.04}$	>230	>189	>212	$0.43^{+0.35}_{-0.23}$	$0.23^{+0.27}_{-0.18}$	$0.37^{+0.30}_{-0.19}$
Mrk 926	60201029002	07906401 01	SW	<0.76	<0.53	<0.79	$1.78^{+0.06}_{-0.06}$	$1.70^{+0.05}_{-0.05}$	$1.77^{+0.05}_{-0.05}$	$1.74^{+0.03}_{-0.05}$	$1.78^{+0.05}_{-0.05}$	>184	>159	>189	<0.36	<0.18	<0.29
LCRS B232242.2-384320	80502607002	08408005 01	SW	<0.77	<0.35	<0.42	$1.75^{+0.10}_{-0.09}$	$1.71^{+0.07}_{-0.07}$	$1.78^{+0.07}_{-0.07}$	$1.71^{+0.07}_{-0.06}$	$1.75^{+0.07}_{-0.06}$	>155	>155	>169	<0.71	<0.49	$0.28^{+0.42}_{-0.26}$
RX J1231.6+7044	60701055002	08918040 01	SW	<2.05	<0.59	<0.68	$1.79^{+0.14}_{-0.11}$	$1.69^{+0.09}_{-0.08}$	$1.75^{+0.11}_{-0.08}$	$1.76^{+0.07}_{-0.12}$	$1.78^{+0.04}_{-0.08}$	>122	>91	>133	<0.29	<0.15	<0.19

(To be continued on the next page)

DOI: 10.52396/JUSTC-2023-0160
JUSTC, **2024**, 54(7): 0702

(Continued)

Source	Nu ID	XMM ID	Mode	$N_{\rm H}^{\rm Nu}$ $10^{22}{\rm cm}^{-2}$	$N_{\rm H}^{\rm pn}$ $10^{22}{\rm cm}^{-2}$	$N_{\rm H}^{\rm pn-Cor}$ $10^{22}{\rm cm}^{-2}$	$\Gamma^{\rm Nu}$	$\Gamma^{\rm pn}$	$\Gamma^{\rm pn-Cor}$	$\Gamma^{\rm joint}$	$\Gamma^{\rm joint-Cor}$	$E_{\rm cut}^{\rm Nu}$ (keV)	$E_{\rm cut}^{\rm joint}$ (keV)	$E_{\rm cut}^{\rm joint-Cor}$ (keV)	$R^{\rm Nu}$	$R^{\rm joint}$	$R^{\rm joint-Cor}$
NGC 4579	6020105100 2	0790840201	FF	<2.40	<3.29	<3.70	$1.83^{+0.18}_{-0.16}$	$1.92^{+0.17}_{-0.14}$	$1.99^{+0.16}_{-0.13}$	$1.88^{+0.14}_{-0.13}$	$1.94^{+0.15}_{-0.13}$	>60	>56	>58	<0.99	<1.31	<1.70
MCG +00-58-028	6000114700 2	0743010501	FF	<2.25	$6.77^{+2.35}_{-2.28}$	$7.15^{+2.36}_{-2.28}$	$2.00^{+0.27}_{-0.20}$	$1.66^{+0.10}_{-0.10}$	$1.74^{+0.10}_{-0.10}$	$1.66^{+0.14}_{-0.17}$	$1.74^{+0.12}_{-0.16}$	>97	>29	>33	$1.15^{+2.27}_{-0.99}$	<1.23	<1.46

See Section 3 for the definition of these parameters.

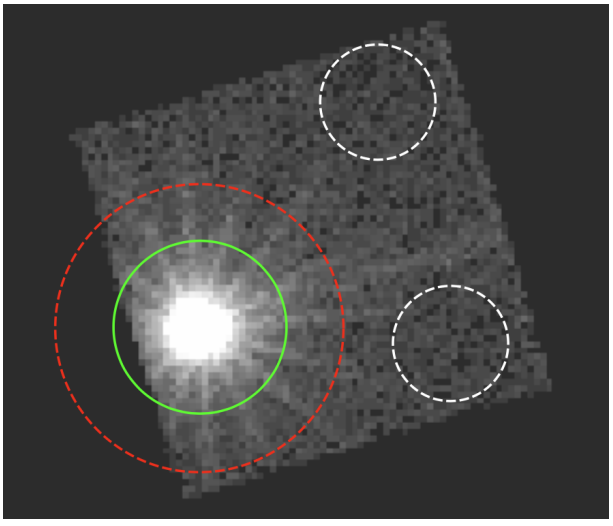

Fig. 1. An example (*XMM-Newton* obsid 0741330101) of the adopted regions when processing the *XMM-Newton* EPIC-pn data in SW mode. The image is extracted at 3–10 keV with *evselect* and plotted in logarithmic scale with *ds9*. The green circle is the source region, which is optimally determined by *eregionanalyse*, while the two white circles with a radius of 40 arcsec are the background regions. Note that part of the source region is outside the FOV (often the case for the SW mode), which will be automatically corrected by *arfgen*. Outside the red circle with a radius of 100 arcsec is the source-free region, used to filter intervals with a flaring background.

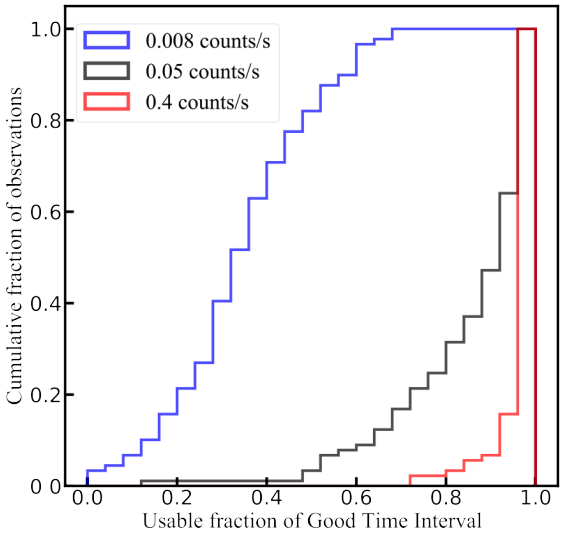

Fig. 2. Usable fraction of the GTI after filtering the periods showing flaring background with different thresholds, for the 85 *XMM-Newton* exposures in SW mode.

to insufficient background subtraction and hence biased spectral parameters. After high background screening, the usable GTI of *NuSTAR* and EPIC-pn are merged to find the overlapped part (see Fig. 3 for an example, and Table 2 for the net exposure time before/after the GTI merge for each *NuSTAR* exposure). The spectra of *NuSTAR* and EPIC-pn for a certain observation pair are then extracted from the overlapped GTI (i.e., with perfect simultaneity). This step is necessary to avoid potential bias caused by rapid X-ray spectral variability of AGN[37], that two spectra without perfect simultaneity may have intrinsically different spectral shape.

3 Spectral fitting

We perform spectral fitting using XSPEC[38] and the χ^2 statistics. All the errors and the upper/lower limits of the parameters are derived following the $\Delta\chi^2 = 2.71$ criterion (corresponding to the 90% confidence level for one interesting parameter). Spectral fitting is carried out in the 3–78 keV band for *NuSTAR* and the 3–10 keV band for EPIC-pn. We drop the EPIC-pn data < 3 keV because to avoid the influence of other spectral components, such as soft X-ray excess and complicated absorption features, in the soft band, and the aforementioned empirical ARF correction for EPIC-pn is available only between 3–12 keV. For each *NuSTAR* observation, the spectra of FPMA and FPMB are jointly fitted with an additional cross-normalization parameter[39].

Following Kang and Wang[9], we employ the model $zphabs\times(pexrav+zgauss)$ to fit the spectra. Among them, *zphabs* models the intrinsic photoelectric absorption, while the Galactic absorption is ignored as it has negligible impact at > 3 keV. *pexrav*[40] models an exponentially cut-off power law with a neutral reflection component, and *zgauss* models the Fe Kα line. During the fitting, the absorption column density $N_{\rm H}$, photon index Γ, high energy cutoff $E_{\rm cut}$, reflection strength R are set free to vary. We deal with the Fe Kα line in the same way as Kang and Wang[9]. We first fix the line at 6.4 keV in the rest frame and the line width at 19 eV (the mean Fe Kα line width in AGNs measured with Chandra HETG[41]) to model a neutral narrow Fe Kα line. Then we set the line width free to vary and adopt the corresponding results if such a variable line width prominently improves the fitting ($\Delta\chi^2 > 5$). To simultaneously show the discrepancy between two missions and how the measurement of $E_{\rm cut}$ and R is affected, we conduct both quasi-independent and joint fit of the *NuSTAR* and EPIC-pn spectra. We firstly fit the *NuSTAR* spectra alone and obtain the best-fit parameters ($\Gamma^{\rm Nu}$, $E_{\rm cut}^{\rm Nu}$, and $R^{\rm Nu}$ in Table 1). Then we fit the corresponding EPIC-

DOI: 10.52396/JUSTC-2023-0160
JUSTC, **2024**, 54(7): 0702

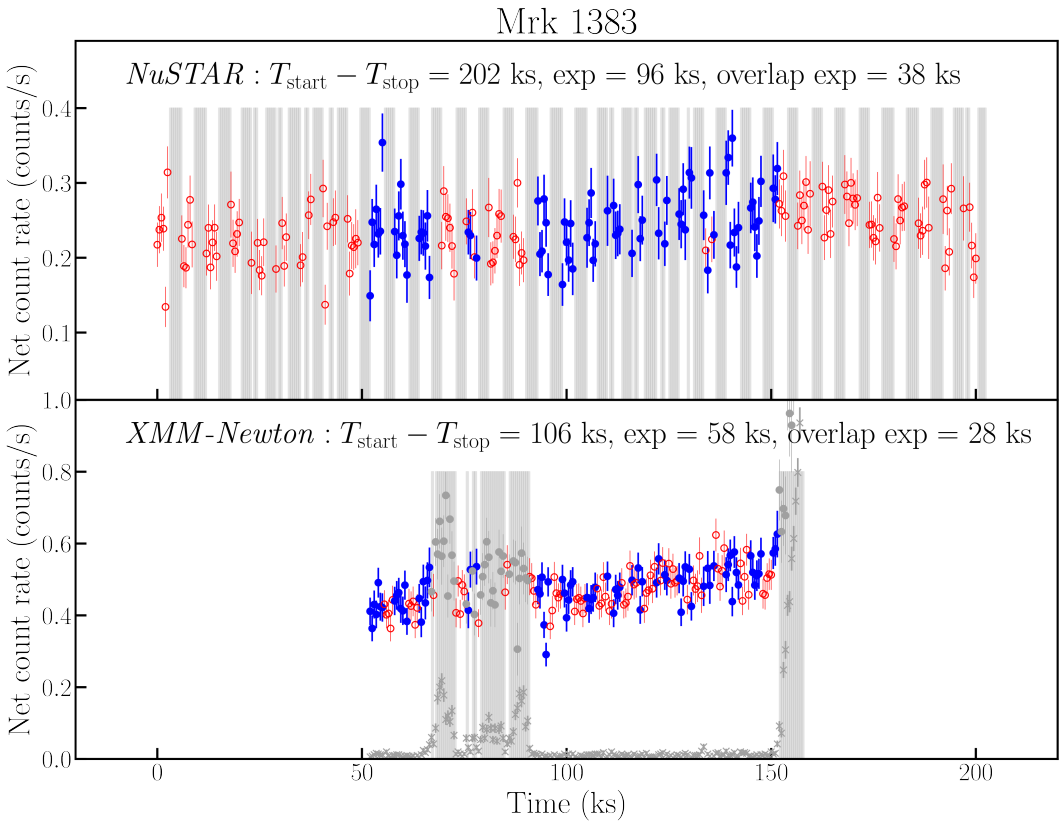

Fig. 3. Example *NuSTAR* FPMA 3–78 keV (ObsID: 60501049002) and *XMM-Newton* EPIC-pn 3–10 keV (ObsID: 0852210101) light curves (with a time bin of 500 s) of Mrk 1383, to illustrate the merge of *NuSTAR* and EPIC-pn GTIs. The grey shades represent the dropped time intervals for each instrument, mainly due to the Earth occultation for *NuSTAR*, and flaring background for EPIC-pn. The blue dots represent the remaining data after merging the GTIs, while the red open circles mark the data dropped due to the merging of GTI. For EPIC-pn (lower panel), we over-plot the background rate curve (grey stars) used to filter the intervals with flaring background, and the corresponding data points filtered out from the source light curve (grey circles). The duration of the exposures and net exposure time (before/after merging GTIs) are labelled, respectively.

Table 2. Fitting results using *NuSTAR* data alone (without requring simultaneity with joint *XMM* exposures).

Source	Nu ID	XMM ID	Nu exp ks	Overlap Nu exp ks	Γ	$E_{\rm cut}$ (keV)	R
Fairall 9	60001130002	0741330101	49.2	3.0	$1.87^{+0.04}_{-0.04}$	> 156	< 1.05
Mrk 359	60402021004	0830550901	49.7	23.6	$1.82^{+0.10}_{-0.09}$	> 109	$0.85^{+0.97}_{-0.58}$
	60402021006	0830551001	51.0	26.9	$1.81^{+0.14}_{-0.07}$	> 205	$0.53^{+0.72}_{-0.43}$
	60402021008	0830551101	48.0	29.1	$1.92^{+0.19}_{-0.20}$	> 85	< 1.97
NGC 931	60101002002	0760530201	63.0	44.6	$1.88^{+0.07}_{-0.07}$	> 253	$0.73^{+0.27}_{-0.23}$
	60101002004	0760530301	64.2	38.7	$1.88^{+0.05}_{-0.06}$	> 343	$0.80^{+0.33}_{-0.25}$
Mrk 1044	60401005002	0824080301	267.1	65.6	$2.49^{+0.05}_{-0.05}$	> 301	$1.75^{+0.61}_{-0.50}$
3C 109	60301011002	0795600101	67.7	28.1	$1.73^{+0.20}_{-0.17}$	> 83	< 0.60
NGC 1566	80301601002	0800840201	56.8	46.4	$1.83^{+0.05}_{-0.05}$	> 453	$0.74^{+0.16}_{-0.15}$
	80401601002	0820530401	75.4	52.7	$1.78^{+0.07}_{-0.07}$	> 352	$0.67^{+0.29}_{-0.25}$
	80502606002	0840800401	57.3	44.7	$1.75^{+0.09}_{-0.14}$	> 190	$0.42^{+0.36}_{-0.28}$
1H 0419-577	60402006002	0820360101	64.2	31.1	$1.67^{+0.13}_{-0.13}$	76^{+55}_{-23}	< 0.55
	60402006004	0820360201	48.3	20.7	$1.59^{+0.11}_{-0.06}$	76^{+34}_{-21}	< 0.52
Ark 120	60001044002	0693781501	55.3	42.5	$1.82^{+0.07}_{-0.04}$	> 557	$0.49^{+0.27}_{-0.17}$
	60001044004	0721600401	65.5	52.0	$1.97^{+0.03}_{-0.03}$	> 588	$0.69^{+0.18}_{-0.18}$
ESO 362-18	60201046002	0790810101	101.9	58.2	$1.55^{+0.09}_{-0.08}$	130^{+97}_{-40}	$0.56^{+0.39}_{-0.31}$
2MASX J05210136-2521450	60201022002	0790580101	155.1	37.0	$2.13^{+0.10}_{-0.09}$	> 218	< 0.87
Mrk 79	60601010004	0870880101	38.5	13.5	$1.80^{+0.05}_{-0.05}$	201^{+523}_{-86}	$0.62^{+0.61}_{-0.42}$

(To be continued on the next page)

DOI: 10.52396/JUSTC-2023-0160
JUSTC, **2024**, 54(7): 0702

(Continued)

Source	Nu ID	XMM ID	Nu exp ks	Overlap Nu exp ks	Γ	$E_{\rm cut}$ (keV)	R
Mrk 110	60502022002	0852590101	86.8	10.8	$1.80^{+0.06}_{-0.06}$	188^{+246}_{-69}	< 0.39
	60502022004	0852590201	88.7	24.5	$1.78^{+0.06}_{-0.06}$	> 166	$0.38^{+0.37}_{-0.30}$
NGC 2992	90501623002	0840920301	57.5	53.1	$1.67^{+0.04}_{-0.04}$	351^{+476}_{-129}	< 0.16
MCG -05-23-016	60701014002	0890670101	83.7	37.7	$1.85^{+0.03}_{-0.03}$	118^{+20}_{-15}	$0.77^{+0.17}_{-0.15}$
NGC 3227	60202002002	0782520201	49.8	25.7	$1.73^{+0.07}_{-0.07}$	165^{+97}_{-46}	$1.20^{+0.40}_{-0.33}$
	60202002004	0782520301	42.5	23.4	$1.61^{+0.09}_{-0.04}$	113^{+58}_{-29}	$0.88^{+0.41}_{-0.33}$
	60202002006	0782520401	39.7	30.3	$1.83^{+0.08}_{-0.08}$	> 206	$0.94^{+0.32}_{-0.27}$
	60202002008	0782520501	41.8	32.7	$1.89^{+0.04}_{-0.03}$	> 652	$0.89^{+0.25}_{-0.23}$
	60202002010	0782520601	40.9	39.1	$1.80^{+0.07}_{-0.05}$	232^{+257}_{-80}	$0.94^{+0.26}_{-0.23}$
	60202002012	0782520701	39.3	29.5	$1.92^{+0.03}_{-0.07}$	> 347	$1.06^{+0.33}_{-0.28}$
	80502609002	0844341301	28.8	25.7	$1.67^{+0.10}_{-0.10}$	> 131	$0.33^{+0.25}_{-0.21}$
	80502609004	0844341401	27.7	20.4	$1.50^{+0.19}_{-0.19}$	> 67	$0.68^{+0.77}_{-0.51}$
2MASSi J1031543-141651	60701046002	0890410101	226.9	47.9	$1.80^{+0.04}_{-0.03}$	159^{+63}_{-39}	$0.70^{+0.41}_{-0.33}$
NGC 3516	60160001002	0854591101	39.9	7.8	$1.96^{+0.06}_{-0.07}$	> 656	$0.77^{+0.69}_{-0.50}$
HE 1136-2304	80002031002	0741260101	23.8	23.7	$1.79^{+0.14}_{-0.16}$	> 92	< 0.79
	80002031003	0741260101	63.6	23.0	$1.60^{+0.05}_{-0.05}$	92^{+78}_{-29}	< 0.50
KUG 1141+371	90601618002	0871190101	38.6	9.7	$1.82^{+0.14}_{-0.09}$	> 73	$0.94^{+1.50}_{-0.88}$
2MASX J11454045-1827149	60302002002	0795580101	21.0	16.7	$1.77^{+0.13}_{-0.13}$	85^{+105}_{-31}	$0.51^{+0.51}_{-0.39}$
	60302002004	0795580201	20.8	12.0	$1.73^{+0.14}_{-0.11}$	> 72	< 0.84
	60302002006	0795580301	23.1	15.1	$1.75^{+0.06}_{-0.06}$	91^{+60}_{-26}	< 0.64
	60302002008	0795580401	20.7	14.3	$1.77^{+0.15}_{-0.10}$	122^{+282}_{-52}	$0.43^{+0.50}_{-0.39}$
	60302002010	0795580501	22.4	13.8	$1.79^{+0.13}_{-0.11}$	> 79	$0.50^{+0.56}_{-0.49}$
NGC 4051	60401009002	0830430201	311.1	31.5	$2.04^{+0.03}_{-0.03}$	> 2384	$1.67^{+0.60}_{-0.48}$
NGC 4593	60001149002	0740920201	23.3	8.1	$1.86^{+0.09}_{-0.08}$	> 269	$0.88^{+0.92}_{-0.54}$
	60001149004	0740920301	21.7	4.6	$1.78^{+0.11}_{-0.11}$	> 543	< 1.42
	60001149006	0740920401	21.3	11.2	$1.72^{+0.07}_{-0.07}$	> 292	$1.18^{+0.89}_{-0.56}$
	60001149008	0740920501	23.1	8.0	$1.82^{+0.05}_{-0.05}$	> 1291	$0.67^{+0.49}_{-0.35}$
	60001149010	0740920601	21.2	12.3	$1.83^{+0.09}_{-0.08}$	> 186	$0.40^{+0.46}_{-0.31}$
MCG -06-30-015	60001047003	0693781301	127.2	64.1	$2.27^{+0.02}_{-0.04}$	> 736	$1.75^{+0.35}_{-0.31}$
	60001047005	0693781401	29.6	15.1	$2.15^{+0.04}_{-0.11}$	> 295	$1.87^{+0.88}_{-0.66}$
IC 4329A	60702050002	0862090101	20.6	6.7	$1.77^{+0.06}_{-0.06}$	> 201	$0.58^{+0.33}_{-0.27}$
	60702050004	0862090301	20.1	6.2	$1.70^{+0.07}_{-0.07}$	> 206	< 0.54
	60702050006	0862090501	19.8	11.0	$1.83^{+0.02}_{-0.07}$	> 404	$0.26^{+0.20}_{-0.17}$
	60702050010	0862090901	18.0	1.2	$1.78^{+0.07}_{-0.07}$	> 171	< 2.46
NGC 5548	60002044003	0720110601	27.3	27.2	$1.77^{+0.08}_{-0.08}$	> 192	$0.64^{+0.26}_{-0.22}$
	60002044005	0720111001	49.5	28.7	$1.55^{+0.03}_{-0.08}$	86^{+20}_{-17}	$0.46^{+0.22}_{-0.20}$
	60002044008	0720111501	50.1	24.5	$1.49^{+0.07}_{-0.07}$	89^{+26}_{-17}	$0.38^{+0.24}_{-0.21}$
ESO 511-G030	60502035002	0852010101	32.1	16.5	$1.70^{+0.09}_{-0.26}$	> 40	< 1.51
	60502035004	0852010201	34.1	18.0	$1.71^{+0.20}_{-0.27}$	> 48	< 0.37
	60502035006	0852010301	31.2	17.4	$1.56^{+0.14}_{-0.11}$	> 57	< 0.29
	60502035008	0852010401	41.8	19.8	$1.64^{+0.09}_{-0.10}$	> 76	< 1.23
Mrk 1383	60501049002	0852210101	96.0	38.0	$1.88^{+0.07}_{-0.07}$	> 142	$0.55^{+0.63}_{-0.42}$
Mrk 817	60702008002	0882340601	65.0	57.8	$2.16^{+0.06}_{-0.08}$	> 1150	$1.57^{+0.54}_{-0.44}$
	60702008004	0882340701	71.7	52.4	$1.74^{+0.14}_{-0.14}$	120^{+176}_{-47}	$0.95^{+0.60}_{-0.45}$

(To be continued on the next page)

DOI: 10.52396/JUSTC-2023-0160
JUSTC, **2024**, 54(7): 0702

(Continued)

Source	Nu ID	XMM ID	Nu exp ks	Overlap Nu exp ks	Γ	$E_{\rm cut}$ (keV)	R
	60702008006	0882340801	78.0	52.1	$1.95^{+0.09}_{-0.16}$	>267	$1.65^{+0.91}_{-0.42}$
Mrk 841	60101023002	0763790501	23.4	8.9	$1.83^{+0.12}_{-0.10}$	>127	$0.99^{+1.28}_{-0.70}$
	60702007002	0882130301	179.6	59.5	$1.87^{+0.07}_{-0.07}$	275^{+577}_{-116}	$0.95^{+0.51}_{-0.41}$
	80701616002	0890640201	53.1	28.0	$1.95^{+0.11}_{-0.12}$	>158	$1.19^{+0.79}_{-0.57}$
3C 382	60202015002	0790600101	23.1	9.5	$1.75^{+0.07}_{-0.08}$	>133	<0.63
	60202015004	0790600201	24.6	12.2	$1.70^{+0.04}_{-0.04}$	115^{+67}_{-31}	<0.58
	60202015006	0790600301	20.8	9.0	$1.74^{+0.04}_{-0.04}$	350^{+455}_{-196}	<0.27
	60202015008	0790600401	21.7	10.6	$1.69^{+0.10}_{-0.07}$	168^{+489}_{-73}	<0.37
	60202015010	0790600501	21.1	8.3	$1.77^{+0.03}_{-0.04}$	>253	<0.26
Fairall 49	60301028002	0795690101	97.8	27.2	$2.42^{+0.07}_{-0.07}$	182^{+442}_{-78}	$1.43^{+0.74}_{-0.57}$
2MASX J19373299-0613046	60101003002	0761870201	65.5	64.0	$2.41^{+0.10}_{-0.10}$	>118	$1.83^{+0.74}_{-0.61}$
	60702018004	0891010201	150.0	55.1	$2.38^{+0.06}_{-0.06}$	>224	$0.78^{+0.43}_{-0.34}$
NGC 6814	60701012002	0885090101	128.2	42.0	$1.83^{+0.03}_{-0.04}$	>644	$0.46^{+0.24}_{-0.20}$
SWIFT J212745.6+565636	60001110002	0693781701	49.2	46.6	$1.88^{+0.08}_{-0.06}$	61^{+15}_{-10}	$1.39^{+0.46}_{-0.35}$
	60001110003	0693781701	28.8	26.5	$1.96^{+0.12}_{-0.12}$	94^{+63}_{-28}	$1.43^{+0.56}_{-0.45}$
	60001110005	0693781801	74.6	67.0	$2.00^{+0.07}_{-0.07}$	87^{+25}_{-16}	$1.73^{+0.36}_{-0.32}$
	60001110007	0693781901	42.1	38.4	$1.96^{+0.08}_{-0.09}$	59^{+19}_{-9}	$1.71^{+0.44}_{-0.38}$
2MASX J21344509-2725557	60363005002	0802200201	21.1	12.3	$1.74^{+0.28}_{-0.13}$	>45	$0.75^{+1.30}_{-0.74}$
NGC 7314	60201031002	0790650101	100.4	30.1	$2.05^{+0.05}_{-0.05}$	345^{+580}_{-138}	$1.00^{+0.36}_{-0.30}$
Mrk 915	60002060002	0744490401	53.0	36.9	$1.80^{+0.12}_{-0.09}$	>365	<0.61
	60002060004	0744490501	54.2	18.1	$1.54^{+0.13}_{-0.13}$	>69	<0.62
	60002060006	0744490601	50.7	7.8	$1.62^{+0.19}_{-0.20}$	>65	<3.43
MR 2251-178	60102025002	0763920501	23.1	5.6	$1.67^{+0.06}_{-0.07}$	137^{+148}_{-53}	<0.10
	60102025004	0763920601	23.2	12.7	$1.75^{+0.07}_{-0.07}$	175^{+263}_{-66}	<0.46
	60102025006	0763920701	20.6	10.6	$1.82^{+0.08}_{-0.08}$	128^{+118}_{-43}	$0.30^{+0.34}_{-0.28}$
	60102025008	0763920801	21.7	10.2	$1.79^{+0.10}_{-0.10}$	171^{+437}_{-71}	$0.32^{+0.37}_{-0.31}$
	90601637002	0872390801	23.6	15.9	$1.63^{+0.11}_{-0.10}$	106^{+174}_{-42}	<0.51
NGC 7469	60101001002	0760350201	21.6	21.4	$1.92^{+0.13}_{-0.08}$	>119	$0.67^{+0.39}_{-0.30}$
	60101001004	0760350301	20.0	19.9	$1.86^{+0.09}_{-0.08}$	>222	$0.48^{+0.36}_{-0.26}$
	60101001006	0760350401	22.5	16.8	$1.88^{+0.06}_{-0.05}$	>312	$0.72^{+0.42}_{-0.30}$
	60101001010	0760350601	20.9	10.7	$1.84^{+0.05}_{-0.05}$	>304	$0.32^{+0.40}_{-0.26}$
	60101001012	0760350701	21.0	10.5	$1.84^{+0.05}_{-0.05}$	>768	$0.96^{+0.55}_{-0.40}$
	60101001014	0760350801	23.4	15.8	$1.83^{+0.05}_{-0.05}$	>201	$0.43^{+0.35}_{-0.23}$
Mrk 926	60201029002	0790640101	106.2	6.1	$1.72^{+0.02}_{-0.02}$	296^{+196}_{-86}	<0.36
LCRS B232242.2-384320	80502607002	0840800501	54.8	38.6	$1.74^{+0.08}_{-0.07}$	>196	<0.71
RX J1231.6+7044	60701055002	0891804001	136.5	18.2	$1.77^{+0.04}_{-0.06}$	>229	<0.29
NGC 4579	60201051002	0790840201	117.8	8.1	$1.81^{+0.04}_{-0.05}$	>125	<0.09
MCG +00-58-028	60001147002	0743010501	26.7	8.3	$1.96^{+0.15}_{-0.12}$	>232	$1.15^{+2.27}_{-0.99}$

"*Nu* exp" refers to the net exposure time of *NuSTAR* FPMA using all available GTI, while "Overlap *Nu* exp" refers to the remaining net exposure after combining the *NuSTAR* GTI with the EPIC-pn GTI of the joint XMM observation. The fitting results in this table are derived with all the available *NuSTAR* data ("*Nu* exp"), not requiring simultaneity with corresponding EPIC-pn exposure.

pn spectrum, with $E_{\rm cut}$ and R fixed at the best-fit results of *NuSTAR* spectra, as both parameters are barely constrained by EPIC-pn data because of the energy-band coverage. We then derive $\Gamma^{\rm pn}$ and $\Gamma^{\rm pn-Cor}$, for effective area uncorrected/corrected EPIC-pn data respectively, to highlight the effect of the calibration issue and the correction. Finally, we jointly fit the *NuSTAR* and EPIC-pn spectra to measure the $E_{\rm cut}^{\rm joint}$, $R^{\rm joint}$, $E_{\rm cut}^{\rm joint-Cor}$, and $R^{\rm joint-Cor}$. During the joint-fitting, all the paramet-

DOI: 10.52396/JUSTC-2023-0160
JUSTC, **2024**, 54(7): 0702

ers of the EPIC-pn spectrum are linked with *NuSTAR* spectra, except a variable constant to account for the absolute normalization between the two missions.

4 Discussion

4.1 The calibration between *NuSTAR* and *XMM-Newton*

We show the best-fit Γ of *NuSTAR* and EPIC-pn spectra in Fig. 4. Patently, the EPIC-pn spectra without the correction are systematically and significantly harder than the coordinated *NuSTAR* spectra. Specifically, we find that mean $\Gamma^{\rm Nu} = 1.84 \pm 0.02$, while the mean $\Gamma^{\rm pn} = 1.74 \pm 0.02$. Meanwhile, the empirical correction of the effective area seems able to completely erase the discrepancy, resulting in the mean $\Gamma^{\rm pn-Cor} = 1.84 \pm 0.02$. Furthermore, the two subsamples of observations before/after 2017-01-01 (roughly equally divided) show that the discrepancy does not evolve with time. We also examine whether the calibration affects the measurement of $N_{\rm H}$. Because we only adopt spectra above 3 keV, for most of the sources $N_{\rm H}$ is not detected and only upper limit could be derived (see Table 1). Adopting *asurv*[42] to handle the upper limits to $N_{\rm H}$, we show in Fig. 5 that before applying the correction, fitting 3–10 keV *XMM* spectra would yield systematically smaller N_H than *NuSTAR*, while applying the correction would also erase the discrepancy.

In Fig. 6 we compare the joint-fitting derived Γ, $E_{\rm cut}$, and R (before and after applying the correction respectively) with those derived through fitting *NuSTAR* spectra alone. Apparently, the smaller Γ also leads to smaller $E_{\rm cut}$ and R when perform joint-fitting, due to the strong positive degeneracy between Γ and $E_{\rm cut}$ as well as between Γ and R[20, 26, 43, 44]. We calculate the mean values of $E_{\rm cut}$ and R using the Kaplan–Meier estimator within *asurv* in logarithm space, obtaining a mean $E_{\rm cut}^{\rm Nu} = 366^{+54}_{-47}$ keV and $R^{\rm Nu} = 0.57^{+0.06}_{-0.06}$, while a mean $E_{\rm cut}^{\rm joint} = 255^{+44}_{-37}$ keV and $R^{\rm joint} = 0.38^{+0.06}_{-0.05}$, with 1σ uncertainty derived through bootstrapping the sample. Meanwhile, the correction is also highly effective for these two parameters, leading to a mean $E_{\rm cut}^{\rm joint-Cor} = 338^{+56}_{-48}$ keV and $R^{\rm joint-Cor} = 0.55^{+0.04}_{-0.04}$.

Therefore, without the correction, the calibration issue between *NuSTAR* and EPIC-pn will bias the measured $E_{\rm cut}$ and R towards lower values. We note the exact strength of the bias would depend on the statistical significance of the EPIC-pn data. Note in this work we require a perfect simultaneity between *NuSTAR* and EPIC-pn data to avoid additional bias due to intrinsic spectral variation, which is not the case in most works. Neglecting the intrinsic variability, the effect of the bias would be stronger if the EPIC-pn exposure is longer than the *NuSTAR* one, as relatively longer EPIC-pn exposure could enhance the dominance of the uncorrected EPIC-pn spectrum's contribution to the joint fitting. Besides, for sources at high redshift or with high accretion rate and very steep spectra[45–47], the bias is also expected to be more serious as the EPIC-pn data could be more dominant during the spectral fitting in these cases. We therefore urge the community to adopt the *XMM-Newton* ARF correction when joint-fitting *XMM-NuSTAR* spectra (but note the correction at < 3 keV is yet unavailable).

Moreover, although in this work we focus on how the measurements of Γ, $E_{\rm cut}$, and R are biased, the calibration issue could also bias the measurements of other parameters derived though joint fitting, for example, the spin of the black-hole a[48–50] and the absorption column density $N_{\rm H}$ in Compton-thick sources[51–53]. Compared with $E_{\rm cut}$ and R, deriving these parameters is more model-dependent and the effect of the bias should be inspected case by case (which is beyond the scope of this work).

4.2 Filter the flaring background of *XMM-Newton* in small window mode

Using *NuSTAR* spectra as references for ARF corrected *XMM-Newton* EPIC-pn spectra, we investigate how the choice of the threshold count rate to filter high background flares affects the spectral fitting results. For the *XMM-Newton* SW mode observations, we now take a threshold of 0.4 counts/s to filter high background intervals, regenerate the common GTI, and in which we extract the corresponding *NuSTAR* and EPIC-pn spectra. To highlight the impact of the flaring background, we limit the comparison to the observations with significant background flaring, through requiring that in > 10% of all usable GTI, the 10–12 keV count rate of the light curve we generated to filter background flares lies between 0.05 counts/s

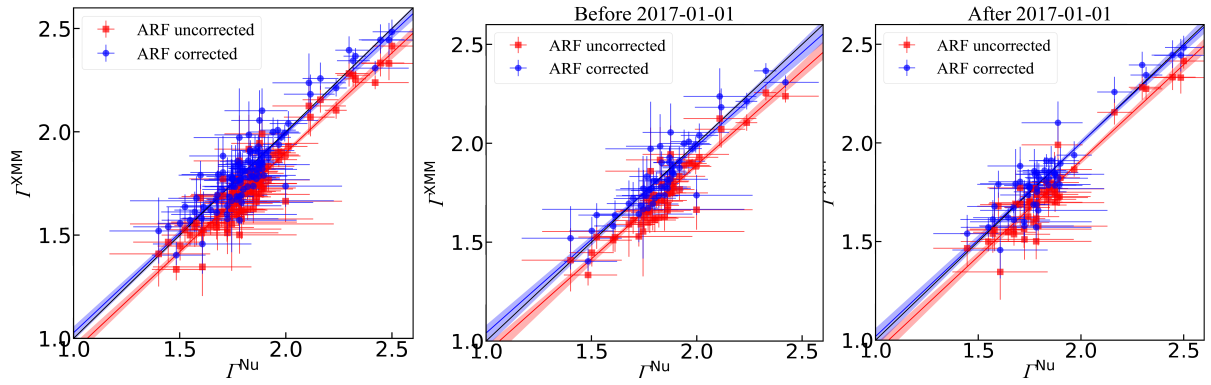

Fig. 4. The left panel: photon index Γ of the *NuSTAR* spectra versus those of the EPIC-pn spectra before (red square) or after (blue circle) correcting the effective area (corresponding to $\Gamma^{\rm Nu}$, $\Gamma^{\rm pn}$, and $\Gamma^{\rm pn-Cor}$ in Table 1, respectively). The colored solid lines show the linear regression results (in comparison with the black 1 : 1 line), with the shadows showing the 1σ uncertainty derived through bootstrapping the sample. The middle and right panels show the case for observations before/after 2017-01-01.

DOI: 10.52396/JUSTC-2023-0160
JUSTC, **2024**, 54(7): 0702

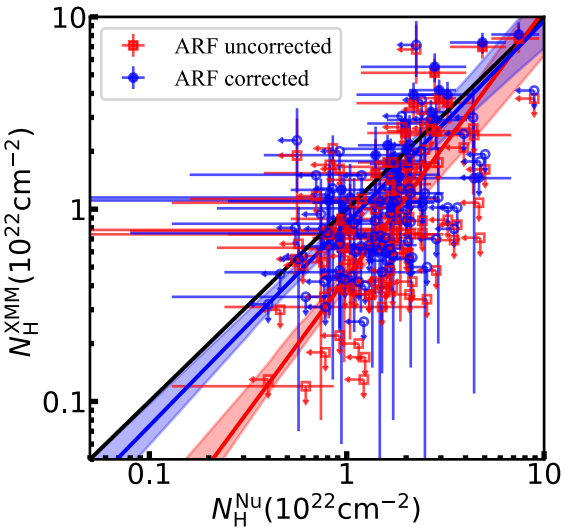

Fig. 5. Absorption column density $N_{\rm H}$ of the *NuSTAR* spectra versus those of the EPIC-pn spectra before (red square) or after (blue circle) correcting the effective area. The colored solid lines show the linear regression results derived by *asurv* (in comparison with the black 1∶1 line), with the shadows showing the 1σ uncertainty derived through bootstrapping the sample.

and 0.4 counts/s. 33 of the 89 SW observations pairs meet this criterion, the $\Gamma^{\rm Nu}$ versus $\Gamma^{\rm pn-Cor}$ of which are shown in Fig. 7.

After applying the *XMM-Newton* released ARF correction, the *XMM-Newton* EPIC-pn spectra generated with a filtering threshold of 0.4 counts/s are still slightly harder than the *NuSTAR* ones (see Fig. 7), with mean $\Gamma^{\rm Nu}_{\rm 0.4\,counts/s} = 1.85 \pm 0.03$ while $\Gamma^{\rm pn-Cor}_{\rm 0.4\,counts/s} = 1.79 \pm 0.03$, indicating the fitting is biased. We interpret the bias as an underestimation of the flaring (soft protons induced) background, as their spectra are apparently much harder than those of AGN (see Section 4 in Ref. [54]), the underestimation of which will hence lead to a harder net spectrum. For SW observations, the target object is always placed near the aim point of the telescope, where the flaring background will be stronger than that in the region used for background subtraction, due to the vignetting effect of the background flares (see Fig. 17 in Ref. [54]). Our finding shows that despite the small FOV of the SW mode, the spatial unevenness of the background is non-negligible when the flaring background is strong and not properly filtered, which will bias the spectral fitting even for these bright AGN.

On the other hand, Fig. 7 also confirms that a threshold of 0.05 counts/s is appropriate to filter high background flares in the SW mode of *XMM-Newton* EPIC-pn observations. After filtering background flares, the residual quiescent soft protons induced background, along with other potential components[55], cause no significant bias at least for these bright AGN.

4.3 Do simultaneous *XMM-Newton* data really help?

As shown above, applying the *XMM-Newton* released ARF correction is highly effective, making the joint-fitting of *NuSTAR* and *XMM-Newton* spectra valid and feasible. However, compared with Kang and Wang[9] which fits the *NuSTAR* spectra alone, it seems that the joint-fitting in this work does not significantly improve the constraints to the spectral parameters. Due to various observational restrictions, the proposed coordinated observations of *NuSTAR* and *XMM-Newton* often can not perfectly overlap (see Fig. 3). Moreover, filtering the periods with flaring background for *XMM-Newton* also loses exposure time (see also Fig. 3). Therefore, if one requires a perfect simultaneity between *NuSTAR* and *XMM-Newton* data as this work does, the involvement of *XMM-Newton* data leads to loss of *NuSTAR* exposure time and hence does not always improve the fitting. As shown in Table 2 and Fig. 8, about 50% of the observations will lose more than 50% of the *NuSTAR* exposure time, if requiring a perfect simultaneity between *NuSTAR* and *XMM-Newton* data. We illustrate an example of Mrk 1383 in Fig. 3, of which a 100 ks coordinated *NuSTAR* and *XMM-Newton* observation was proposed. We first note that for a long *NuSTAR* observation in science mode, only about 50% of the duration time is available for exposure due to the Earth occultation. Therefore, a proposed 100 ks *NuSTAR* exposure is acutally discontinuously distributed in a ~ 200 ks duration, indicating it can never be perfectly simultaneous with a 100 ks long *XMM-Newton* exposure. In the example we show in Fig. 3 for Mrk 1383, the unique distribution of *NuSTAR* exposure directly causes a loss of ~ 50% net exposure time for both *NuSTAR* and *XMM-Newton* if requiring a perfect simultaneity. Furthermore, filtering the intervals with flaring background for *XMM-Newton* causes a further loss of the exposure time. Taken together, inclusion of the *XMM-Newton* data

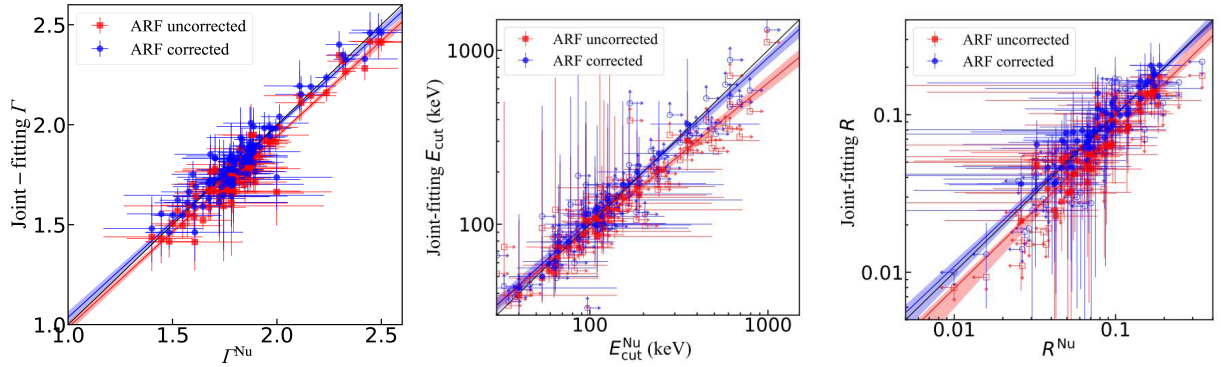

Fig. 6. Γ, $E_{\rm cut}$ and R derived through fitting the *NuSTAR* spectra alone versus joint-fitting with EPIC-pn spectra. For $E_{\rm cut}$ and R, we perform linear regression in logarithmic space with *asurv*[42] to handle the censored data points (as hollow markers). The colored solid lines show the linear regression results (in comparison with the black 1∶1 line), with the shadow showing the 1σ uncertainty derived through bootstrapping the sample.

DOI: 10.52396/JUSTC-2023-0160
JUSTC, **2024**, 54(7): 0702

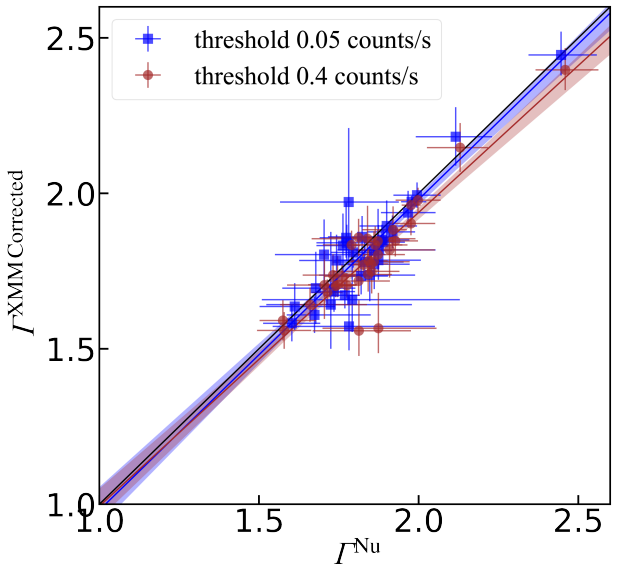

Fig. 7. The photon index Γ (y-axis) derived using the effective area corrected *XMM-Newton* EPIC-pn spectra, after filtering the periods showing flaring background with a threshold of 0.05 counts/s (blue squares) or 0.4 counts/s (brown circles), versus those derived using *NuSTAR* spectra (x-axis), for the 33 observation pairs with significant flaring background. The colored solid lines show the linear regression results (in comparison with the black 1∶1 line), with the shadow showing the 1σ uncertainty derived through bootstrapping the sample.

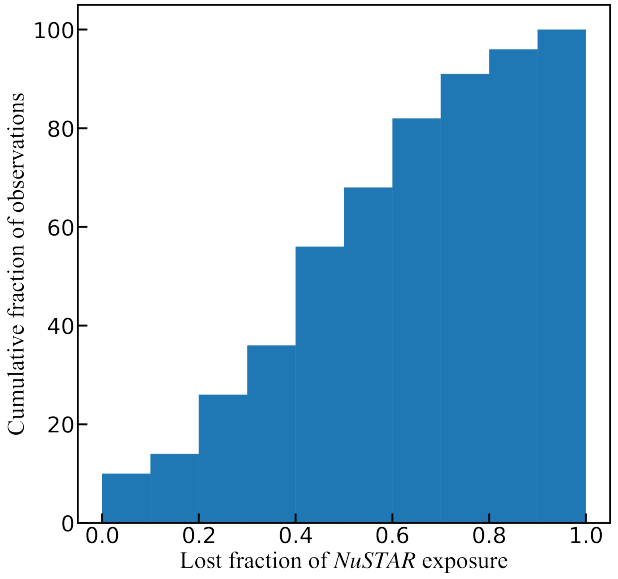

Fig. 8. Lost fraction of the *NuSTAR* net exposure after requiring a perfect simultaneity between *NuSTAR* and *XMM-Newton* data.

causes a loss of more than 60% of the *NuSTAR* net exposure time. Note for the Small Window mode of EPIC-pn, the live-time fraction is only 71%. This leads to a shorter net exposure time of *XMM-Newton* (28 ks) than *NuSTAR* one (38 ks) after merging the GTIs, which further reduces the statistical significance of *XMM-Newton* data.

To conduct a quantified assessment, we extract *NuSTAR* spectra in all the available GTI (without a match with EPIC-pn) and fit them with the same model, the result of which is shown in Table 2. In Fig. 9, we show the distribution of the relative errors of Γ, R and $E_{\rm cut}$, along with the detection fraction of R, and $E_{\rm cut}$. In conclusion, for this sample and this model, the involvement of *XMM-Newton* data does not significantly help.

If we make a concession about the simultaneity, simply including a quasi-simultaneous *XMM-Newton* exposure will certainly improve the constraint of the spectral parameters, which however could bring biases for variable sources like AGN. Moreover, here we adopt *pexrav*, a simple model without strong physical assumptions, to model the reflection component, while models like *pexmon*[56], *xillver*, and *relxill*[57, 58] perform self-consistently fitting on the reflection component and the Fe Kα line. EPIC spectra will be statistically more significant on the constraint of $E_{\rm cut}$ and R when fitting with these models, as they provide good constraint for the Fe Kα line. However, we stress the coupling between the reflection component and Fe Kα line is yet unclear [19, 59, 60]. Finally, we note the current correction of the effective area is limited to 3–12 keV, indicating the EPIC data below 3 keV are not usable when performing joint-fitting with *NuSTAR*. With proper soft band correction and wider dynamic range, EPIC spectral would be statistically more important, though the complicated absorption and soft excess in the soft band might induce other biases.

5 Summary

In this work we perform joint-fitting of *NuSTAR* and *XMM-Newton* EPIC-pn spectra for a large sample of 104 observation pairs of 44 AGN. Below are our main results.

(Ⅰ) Calibration issue does exist between two missions; EPIC-pn spectra are systematically harder than those of *NuSTAR* ($\Delta\Gamma\sim0.1$), leading to underestimated cutoff energy $E_{\rm cut}$ and reflection component R when performing joint-fitting before correcting the calibration issue.

(Ⅱ) The empirical correction of the effective area implemented in latest *XMM-Newton* calibration files (but would not be applied by default) is highly effective and could commendably erase the discrepancy in the derived best-fit Γ, $E_{\rm cut}$, and R.

(Ⅲ) For this sample, requiring a perfect simultaneity between the *NuSTAR* and EPIC-pn spectra leads to serious loss of net exposure time of *NuSTAR*. Consequently, fitting *NuSTAR* spectra jointly with simultaneous EPIC-pn data does not always improve the constraints to the key spectral parameters.

(Ⅳ) For *XMM-Newton* EPIC-pn observations in Small Window mode, insufficient filtering of high background flares could bias the spectral fitting results due to the background vignetting effect, which is no longer negligible in case of background flares. A threshold of 0.05 counts/s to filter background flares (see Section 2 for the definition) appears appropriate for EPIC-pn SW mode.

Finally, we note again the correction of the effective area is not applied by default in *arfgen*. Since the corresponding corrections to the effective areas in the < 3 keV energies remain unknown, the SAS *applyabsfluxcorr* correction should not be applied if < 3 keV *XMM-Newton* data are included, in joint analysis or analyzing *XMM-Newton* data alone. However, one should always keep in mind there are potential

DOI: 10.52396/JUSTC-2023-0160
JUSTC, **2024**, 54(7): 0702

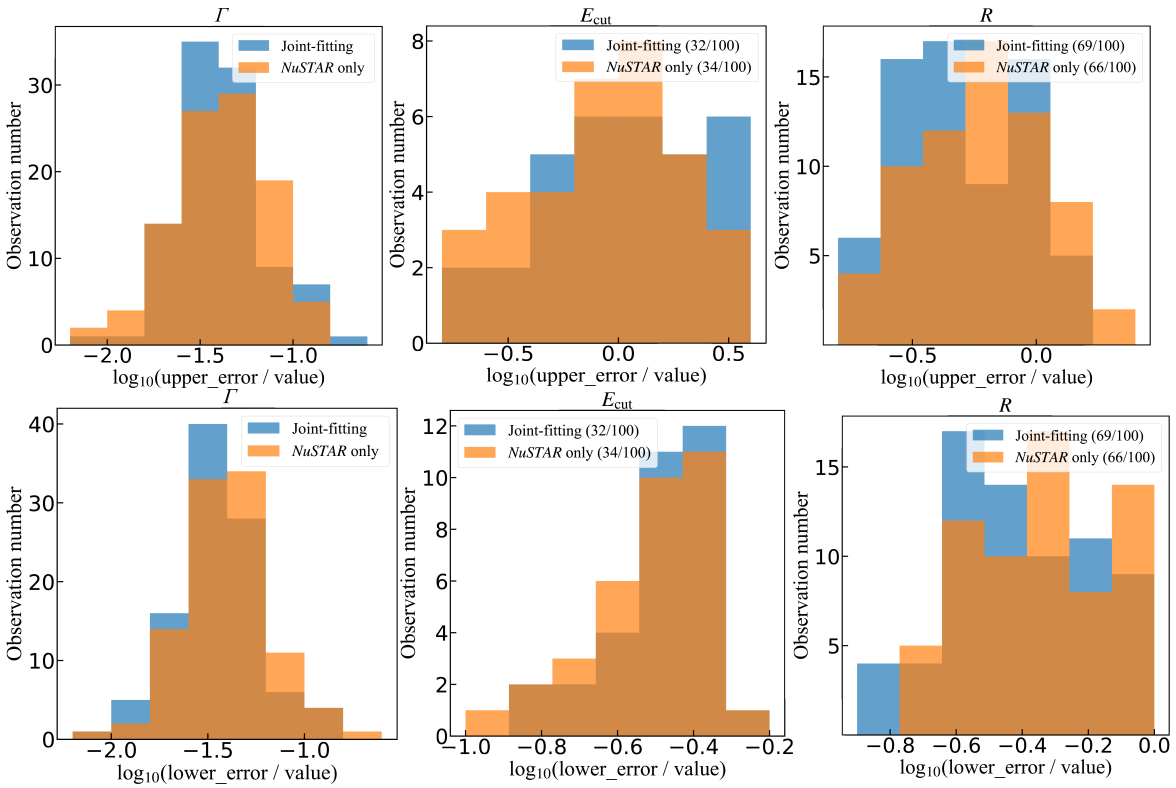

Fig. 9. The distribution of the relative errors of Γ, R and $E_{\rm cut}$, with the detection fraction of R and $E_{\rm cut}$ provided in the legend. The top panels show the distributions of $\log_{10}\left(\frac{\text{upper error}}{\text{value}}\right)$ of the three parameters, while the bottom panels show those of $\log_{10}\left(\frac{\text{lower error}}{\text{value}}\right)$. Blue boxes show the results of the joint-fitting of *NuSTAR* and EPIC-pn, while the orange boxes show the result of fitting the *NuSTAR* spectra only (from the whole *NuSTAR* exposure without matching EPIC-pn GTI).

biases in such cases due to the uncertainties of the calibration, which may hamper accurate measurements of soft excess and ionized absorption, for example. We look forward to an updated correction curve in future calibration releases.

Acknowledgements

We thank the anonymous referees for their highly constructive comments which significantly improved the paper. This research has made use of the *NuSTAR* Data Analysis Software (NuSTARDAS) jointly developed by the ASI Science Data Center (ASDC, Italy) and the California Institute of Technology (USA). This work is based on observations obtained with *XMM-Newton*, an ESA science mission with instruments and contributions directly funded by ESA Member States and NASA. This work was supported by the National Natural Science Foundation of China (12033006, 12192221, 123B2042). The authors gratefully acknowledge the support of Cyrus Chun Ying Tang Foundations.

Conflict of interest

The authors declare that they have no conflict of interest.

Biographies

Jia-Lai Kang is currently a Ph.D. student under the supervision of Professor Jun-Xian Wang at University of Science and Technology of China. His research is focused on active galactic nuclei.

Jun-Xian Wang is currently a Professor at the University of Science and Technology of China (USTC). He received his Ph.D. degree from USTC. His research interests mainly focus on active galactic nuclei and high redshift galaxies.

Preprint statement

Research presented in this article was posted on a preprint server prior to publication in JUSTC. The corresponding preprint article can be found here: https://arxiv.org/abs/2311.15499

References

[1] Harrison F A, Craig W W, Christensen F E, et al. The nuclear spectroscopic telescope array (*NuSTAR*) high-energy X-ray mission. *The Astrophysical Journal*, **2013**, *770*: 103.

[2] Haardt F, Maraschi L. A two-phase model for the X-ray emission from Seyfert galaxies. *The Astrophysical Journal*, **1991**, *380*: L51.

[3] Haardt F, Maraschi L. X-ray spectra from two-phase accretion disks. *The Astrophysical Journal*, **1993**, *413*: 507.

[4] Brenneman L W, Madejski G, Fuerst F, et al. The broad-band X-ray spectrum of ic 4329a from a joint *NuSTAR/Suzaku* observation. *The Astrophysical Journal*, **2014**, *788*: 61.

[5] Matt G, Baloković M, Marinucci A, et al. The hard X-ray spectrum of NGC 5506 as seen by *NuSTAR*. *Monthly Notices of the Royal Astronomical Society*, **2015**, *447*: 3029–3033.

[6] Fabian A C, Lohfink A, Kara E, et al. Properties of AGN coronae in the *NuSTAR* era. *Monthly Notices of the Royal Astronomical Society*, **2015**, *451*: 4375–4383.

[7] Kamraj N, Harrison F, Baloković M, et al. Coronal properties of

DOI: 10.52396/JUSTC-2023-0160
JUSTC, **2024**, 54(7): 0702

Swift/BAT-selected Seyfert 1 AGNs observed with *NuSTAR*. 2018, *866*: 124.

[8] Baloković M, Harrison F A, Madejski G, et al. *NuSTAR* survey of obscured swift/BAT-selected active galactic nuclei. II. Median high-energy cutoff in Seyfert II hard X-ray spectra. *The Astrophysical Journal*, **2020**, *905*: 41.

[9] Kang J L, Wang J X. The X-ray coronae in NuSTAR bright active galactic nuclei. *The Astrophysical Journal*, **2022**, *929*: 141.

[10] Parker M L, Wilkins D R, Fabian A C, et al. The *NuSTAR* spectrum of Mrk 335: extreme relativistic effects within two gravitational radii of the event horizon. *Monthly Notices of the Royal Astronomical Society*, **2014**, *443*: 1723–1732.

[11] Kara E, Zoghbi A, Marinucci A, et al. Iron K and Compton hump reverberation in SWIFT J2127. *4+5654 and NGC 1365 revealed by NuSTAR and XMM–Newton. Monthly Notices of the Royal Astronomical Society*, **2015**, *446*: 737–749.

[12] Wilkins D R, Gallo L C. Driving extreme variability: The evolving corona and evidence for jet launching in Markarian 335. *Monthly Notices of the Royal Astronomical Society*, **2015**, *449*: 129–146.

[13] Panagiotou C, Walter R. Reflection geometries in absorbed and unabsorbed AGN. *Astronomy & Astrophysics*, **2019**, *626*: A40.

[14] Jansen F, Lumb D, Altieri B, et al. XMM-Newton observatory. *Astronomy & Astrophysics*, **2001**, *365*: L1–L6.

[15] Cappi M, De Marco B, Ponti G, et al. Anatomy of the AGN in NGC 5548 VIII. *XMM-Newton's EPIC detailed view of an unexpected variable multilayer absorber. Astronomy & Astrophysics*, **2016**, *592*: A27.

[16] Ponti G, Bianchi S, Muños-Darias T, et al. *NuSTAR + XMM-Newton* monitoring of the neutron star transient AX J1745.6-2901. *Monthly Notices of the Royal Astronomical Society*, **2018**, *473*: 2304–2323.

[17] Middei R, Bianchi S, Petrucci P O, et al. High-energy monitoring of NGC 4593 II. *Broad-band spectral analysis:testing the two-corona model. Monthly Notices of the Royal Astronomical Society*, **2019**, *483*: 4695–4705.

[18] Rani P, Stalin C S, Goswami K D. Study of X-ray variability and coronae of Seyfert galaxies using *NuSTAR*. *Monthly Notices of the Royal Astronomical Society*, **2019**, *484*: 5113–5128.

[19] Kang J, Wang J, Kang W. *NuSTAR* hard X-ray spectra of radio galaxies. *The Astrophysical Journal*, **2020**, *901*: 111.

[20] Panagiotou C, Walter R. *NuSTAR* view of *Swift*/BAT AGN: The *R*–Γ correlation. *Astronomy & Astrophysics*, **2020**, *640*: A31.

[21] Akylas A, Georgantopoulos I. Distribution of the coronal temperature in Seyfert 1 galaxies. *Astronomy & Astrophysics*, **2021**, *655*: A60.

[22] Pal I, Stalin C S. Search for coronal temperature variation in Seyfert galaxies. *Monthly Notices of the Royal Astronomical Society*, **2022**, *518*: 2529–2545.

[23] Marinucci A, Matt G, Kara E, et al. Simultaneous *NuSTAR* and *XMM–Newton* 0.5–80 keV spectroscopy of the narrow-line Seyfert 1 galaxy SWIFT J2127.4+5654. *Monthly Notices of the Royal Astronomical Society*, **2014**, *440*: 2347–2356.

[24] Tortosa A, Bianchi S, Marinucci A, et al. A *NuSTAR* census of coronal parameters in Seyfert galaxies. *Astronomy & Astrophysics*, **2018**, *614*: A37.

[25] Zhang J X, Wang J X, Zhu F F. On measuring the variation of high-energy cutoff in active galactic nuclei. *The Astrophysical Journal*, **2018**, *863*: 71.

[26] Molina M, Malizia A, Bassani L, et al. *Swift*/XRT–*NuSTAR* spectra of type 1 AGN: Confirming INTEGRAL results on the high-energy cut-off. *Monthly Notices of the Royal Astronomical Society*, **2019**, *484*: 2735–2746.

[27] Hinkle J T, Mushotzky R. Fundamental X-ray corona parameters of Swift/BAT AGN. *Monthly Notices of the Royal Astronomical Society*, **2021**, *506*: 4960–4978.

[28] Kamraj N, Brightman M, Harrison F A, et al. X-ray coronal properties of swift/BAT-selected Seyfert 1 active galactic nuclei. *The Astrophysical Journal*, **2022**, *927*: 42.

[29] Pal I, Stalin C S, Parker M L, et al. X-ray spectral and timing analysis of the Compton Thick Seyfert 2 galaxy NGC 1068. *Monthly Notices of the Royal Astronomical Society*, **2022**, *517*: 3341–3353.

[30] Madsen K K, Forster K, Grefenstette B W, et al. Measurement of the absolute crab flux with *NuSTAR*. *The Astrophysical Journal*, **2017**, *841*: 56.

[31] Madsen K K, Forster K, Grefenstette B, et al. Effective area calibration of the Nuclear Spectroscopic Telescope Array. *Journal of Astronomical Telescopes, Instruments, and Systems*, **2022**, *8*: 034003.

[32] Oh K, Koss M, Markwardt C B, et al. The 105-month *Swift*-BAT all-sky hard X-ray survey. *The Astrophysical Journal Supplement Series*, **2018**, *235*: 4.

[33] Strüder L, Briel U, Dennerl K, et al. The European Photon Imaging Camera on *XMM-Newton*: The pn-CCD camera. *Astronomy & Astrophysics*, **2001**, *365*: L18–L26.

[34] Turner M J L, Abbey A, Arnaud M, et al. The European photon imaging camera on XMM-Newton: The mos cameras. *Astronomy and Astrophysics*, **2001**, *365*: L27–L35.

[35] Read A M, Ponman T J. The *XMM-Newton* EPIC background: Production of background maps and event files. *Astronomy & Astrophysics*, **2003**, *409*: 395–410.

[36] Carter J A, Read A M. The *XMM-Newton* EPIC background and the production of background blank sky event files. *Astronomy & Astrophysics*, **2007**, *464*: 1155–1166.

[37] Wu Y J, Wang J X, Cai Z Y, et al. More than softer-when-brighter: The X-ray powerlaw spectral variability in NGC 4051. *Science China Physics, Mechanics & Astronomy*, **2020**, *63*: 129512.

[38] K. A. Arnaud. XSPEC: The first ten years. In: Jacoby G H, Barnes J, editors. Astronomical Data Analysis Software and Systems V, Volume 101 of Astronomical Society of the Pacific Conference Series. San Francisco, USA: Astronomical Society of the Pacific, **1996**: 17.

[39] Madsen K K, Harrison F A, Markwardt C B, et al. Calibration of the *NuSTAR* high-energy focusing x-ray telescope. *The Astrophysical Journal Supplement Series*, **2015**, *220*: 8.

[40] Magdziarz P, Zdziarski A A. Angle-dependent Compton reflection of X-rays and gamma-rays. *Monthly Notices of the Royal Astronomical Society*, **1995**, *273*: 837–848.

[41] Shu X W, Yaqoob T, Wang J X. The cores of the Fe Kα lines in active galactic nuclei: An extended *Chandra* high energy grating sample. *The Astrophysical Journal Supplement Series*, **2010**, *187*: 581.

[42] Feigelson E D, Nelson P I. Statistical methods for astronomical data with upper limits. I - Univariate distributions. *The Astrophysical Journal*, **1985**, *293*: 192–206.

[43] Kang J L, Wang J X, Wen-Yong Kang W Y. Distinct high-energy cutoff variation patterns in two Seyfert galaxies. *Monthly Notices of the Royal Astronomical Society*, **2021**, *502* (1): 80–88.

[44] Kang J L, Wang J X. Hidden biases in flux-resolved X-ray spectroscopy. *Monthly Notices of the Royal Astronomical Society*, **2023**, *519*: 3635–3642.

[45] Lanzuisi G, Perna M, Comastri A, et al. *NuSTAR* reveals the extreme properties of the super-Eddington accreting supermassive black hole in PG 1247+267. *Astronomy & Astrophysics*, **2016**, *590*: A77.

[46] G. Lanzuisi, R, Gilli, M. Cappi, et al. NuSTAR measurement of coronal temperature in two luminous, high-redshift quasars. *The Astrophysical Journal Letters*, **2019**, *875*: L20.

[47] Tortosa A, Ricci C, Tombesi F, et al. The extreme properties of the nearby hyper-Eddington accreting active galactic nucleus in IRAS 04416+1215. *Monthly Notices of the Royal Astronomical Society*, **2021**, *509*: 3599–3615.

[48] Risaliti G, Harrison F A, Madsen K K, et al. A rapidly spinning supermassive black hole at the centre of NGC 1365. *Nature*, **2013**, *494*: 449–451.

DOI: 10.52396/JUSTC-2023-0160
JUSTC, **2024**, 54(7): 0702

[49] Porquet D, Done C, Reeves J N, et al. A deep X-ray view of the bare AGN Ark 120. *Astronomy & Astrophysics*, **2019**, *623*: A11.
[50] Jiang J, Abdikamalov A B, Bambi C, et al. Black hole spin measurements based on a thin disc model with finite thickness–I. An example study of MCG−06-30-15. *Monthly Notices of the Royal Astronomical Society*, **2022**, *514*: 3246–3259.
[51] Marchesi S, Zhao X, Torres-Albà N, et al. Compton-thick AGN in the NuSTAR Era. VIII. A joint NuSTAR–XMM-Newton Monitoring of the Changing-look Compton-thick AGN NGC 1358. *The Astrophysical Journal*, **2022**, *935*: 114.
[52] Silver R, Torres-Albà N, Zhao X, et al. Compton-thick AGN in the *NuSTAR* era. IX. A joint NuSTAR and XMM-newton analysis of four local AGN. *The Astrophysical Journal*, **2022**, *940*: 148.
[53] Sengupta D, Marchesi S, Vignali C, et al. Compton-thick AGN in the *NuSTAR* Era X: analysing seven local CT-AGN candidates. *Astronomy & Astrophysics*, **2023**, *676*: A103.
[54] Kuntz K D, Snowden S L. The EPIC-MOS particle-induced background spectra. *Astronomy & Astrophysics*, **2008**, *478*: 575–596.
[55] De Luca A, Molendi S. The 2–8 keV cosmic X-ray background spectrum as observed with *XMM-Newton*. *Astronomy & Astrophysics*, **2004**, *419*: 837–848.
[56] Nandra K, O'Neill P M, George I M, et al. An XMM–Newton survey of broad iron lines in Seyfert galaxies. *Monthly Notices of the Royal Astronomical Society*, **2007**, *382*: 194–228.
[57] Dauser T, Wilms J, Reynolds C S, et al. Broad emission lines for a negatively spinning black hole. *Monthly Notices of the Royal Astronomical Society*, **2010**, *409*: 1534–1540.
[58] García J, Dauser T, Lohfink A, et al. Improved reflection models of black hole accretion disks: Treating the angular distribution of X-rays. *The Astrophysical Journal*, **2014**, *782*: 76.
[59] Chiang J, Reynolds C S, Blaes O M, et al. Simultaneous *EUVE*/*ASCA*/*RXTE* observations of NGC 5548. *The Astrophysical Journal*, **2000**, *528*: 292–305.
[60] Mantovani G, Nandra K, Ponti G. Relativistic Fe Kα line study in Seyfert 1 galaxies observed with Suzaku. *Monthly Notices of the Royal Astronomical Society*, **2016**, *458*: 4198–4209.

DOI: 10.52396/JUSTC-2023-0160
JUSTC, **2024**, 54(7): 0702